# Relationships between magmatism and deformation in southeastern Proterozoic Australia

Thesis submitted in accordance with the requirements of the University of Adelaide for an Honours Degree in Geology/Geophysics

Adrienne Brotodewo

November 2016


THE UNIVERSITY of ADELAIDE

# CONSTRAINTS ON MESOPROTEROZOIC MAGMATISM AND DEFORMATION IN THE SOUTHERN GAWLER CRATON, SOUTH AUSTRALIA

## MAGMATISM AND DEFORMATION IN YORKE PENINSULA

## ABSTRACT

The ca. 1600–1580 Ma time slice is recognised as a significant period of magmatism and deformation throughout eastern Proterozoic Australia. Within the northern Yorke Peninsula, this period was associated with the emplacement of multiple phases of the Tickera Granite; an intensely foliated orange granite, a white leucogranite and a red granite. These granites belong to the broader Hiltaba Suite that was emplaced at shallow crustal levels, throughout the Gawler Craton. Geochemical and isotopic analysis suggests these granite phases were derived from a heterogeneous source region. The orange and red granites were derived from the Donington Suite and/or the Wallaroo Group metasediments with slight contamination from an Archean basement. The white leucogranite is sourced from a similar but slightly more mafic/lower crustal source. Phases of the Tickera Granite were emplaced synchronously with deformation that resulted in development of a prominent northeast trending structural grain throughout the Yorke Peninsula region. This fabric is a composite of two fold generations; early isoclinal folds that were refolded by later open upright folds. Isoclinal folding may have occurred during the ca. 1730–1690 Ma Kimban Orogeny, or just prior to emplacement of the Tickera Granite at ca. 1597–1577 Ma. The upright fold generation was contemporaneous with the emplacement of the Tickera Granite. The Yorke Peninsula shares a common geological history with the Curnamona Province, which was deformed during the ca. 1600–1585 Ma Olarian Orogeny, and resulted in development of early isoclinal (recumbent) folds overprinted by an upright fold generation, a dominant northeast–trending structural grain and spatially and temporally related intrusions. This suggests that an apparent correlation with the geological history of the Curnamona Province, and that the Olarian Orogeny may have also affected the southeastern Gawler Craton. Constraint on the timing of the earlier isoclinal fold generation in the Yorke Peninsula will allow further understanding of the similarities between the two regions.

## KEYWORDS

Mesoproterozoic; Magmatism; Deformation; Yorke Peninsula; Tickera Granite; Hiltaba Suite; Olarian Orogeny; Gawler Craton; Curnamona Province

**TABLE OF CONTENTS**

## LIST OF FIGURES AND TABLES

## INTRODUCTION

The ca. 1600–1580 Ma time slice is a recognised period of high grade metamorphism associated with intense crustal orogenesis within eastern Proterozoic Australia (e.g. Collins & Shaw 1995; Betts et al., 2002; Forbes et al., 2008; Stewart & Betts 2010; Forbes et al., 2012), which includes the Gawler Craton and Curnamona Province of South Australia (Fig. 1a,b). Within the Gawler Craton, this period was also associated with bimodal volcanism that resulted in outpouring of the ca. 1592 Ma Gawler Range Volcanics (Fanning et al., 1998) and emplacement of the ca. 1595–1575 Ma Hiltaba Suite Granites (e.g. Flint et al., 1993; Conor 1995; Creaser & Cooper 1993; Fanning et al., 2007) to shallow crustal levels (e.g. Daly et al., 1998; Stewart & Foden 2003). The Hiltaba Suite granites are widely distributed across the Gawler Craton and are suggested to comprise two phases emplaced at ca. 1590 Ma and ca. 1580 Ma (Stewart & Foden 2003; Hand et al., 2007). The granites vary across the A-, I- and S-type range, and have characteristic chemical signatures (such as high $SiO_2$: CaO, MnO, Sr ratios and Sm–Nd isotopes) depending on whether they are part of the older or younger phase of granites (Stewart & Foden 2003; Hand et al., 2007).

Granites in the northern Yorke Peninsula in the southern Gawler Craton (Fig. 1c) are suggested to be part of the Hiltaba Suite, and include the deformed Tickera Granite (1598±7 Ma, 1575 ± 7 Ma: Conor 1995) and undeformed Arthurton Granite (1583 ± 7 Ma: Creaser & Cooper 1993). These granites intrude metasediments and metavolcanics of the ca. 1750 Ma Wallaroo Group (Cowley et al., 2003). Magmatic crystallization ages derived from the Tickera Granite range from ca. 1597–1577 Ma (Conor 1995), suggesting variable conditions and timing of emplacement. The timing of emplacement of the Tickera Granite is also synchronous with deformation, metamorphism and

metasomatism that is suggested to have affected the Wallaroo Group at ca. 1600–1575 Ma (Conor et al., 2010). However, details on emplacement relationships and associated events that affected the Yorke Peninsula region is lacking.

This study aims to constrain the relative timing of emplacement of multiple phases of the deformed Tickera Granite exposed at Point Riley in the northwestern Yorke Peninsula and place this in context of the southeastern Proterozoic Australia (Fig. 1c). This has been done through detailed mapping to assess relative intrusive relationships, structural fabrics and deformation styles within the granite phases and comparison with hosting Wallaroo Group metasediments. Whole rock geochemical and Sm–Nd isotopic analysis of the granite phases is used to assess the source region of the multiple phases identified, and place the Tickera Granite within the broader context of the ca. 1595–1575 Ma Hiltaba Suite (Creaser & Cooper 1993; Fanning et al., 2007). The magmatic and deformational history of the Yorke Peninsula is then discussed in relation to the ca. 1600–1585 Ma Olarian Orogeny (Page et al., 2005) that affected eastern Proterozoic Australia, particularly within the Gawler Craton and Curnamona Province.

## REGIONAL GEOLOGY OF THE GAWLER CRATON

The Gawler Craton preserves a complex geological history spanning from the late Archean to the early Mesoproterozoic. Mesoarchean granitoids of the Cooyerdoo Granite were emplaced between ca. 3200–3150 Ma, and are recognised as the oldest known units within the Gawler Craton (Fraser et al., 2010a; Jagodzinski et al., 2011b; Reid & Hand 2012). Felsic magmatism associated with emplacement of the Coolanie Gneiss occurred at ca. 2823 Ma (Fraser and Neumann, 2010), and was followed by bimodal magmatism and sedimentation during the Neoarchean to early

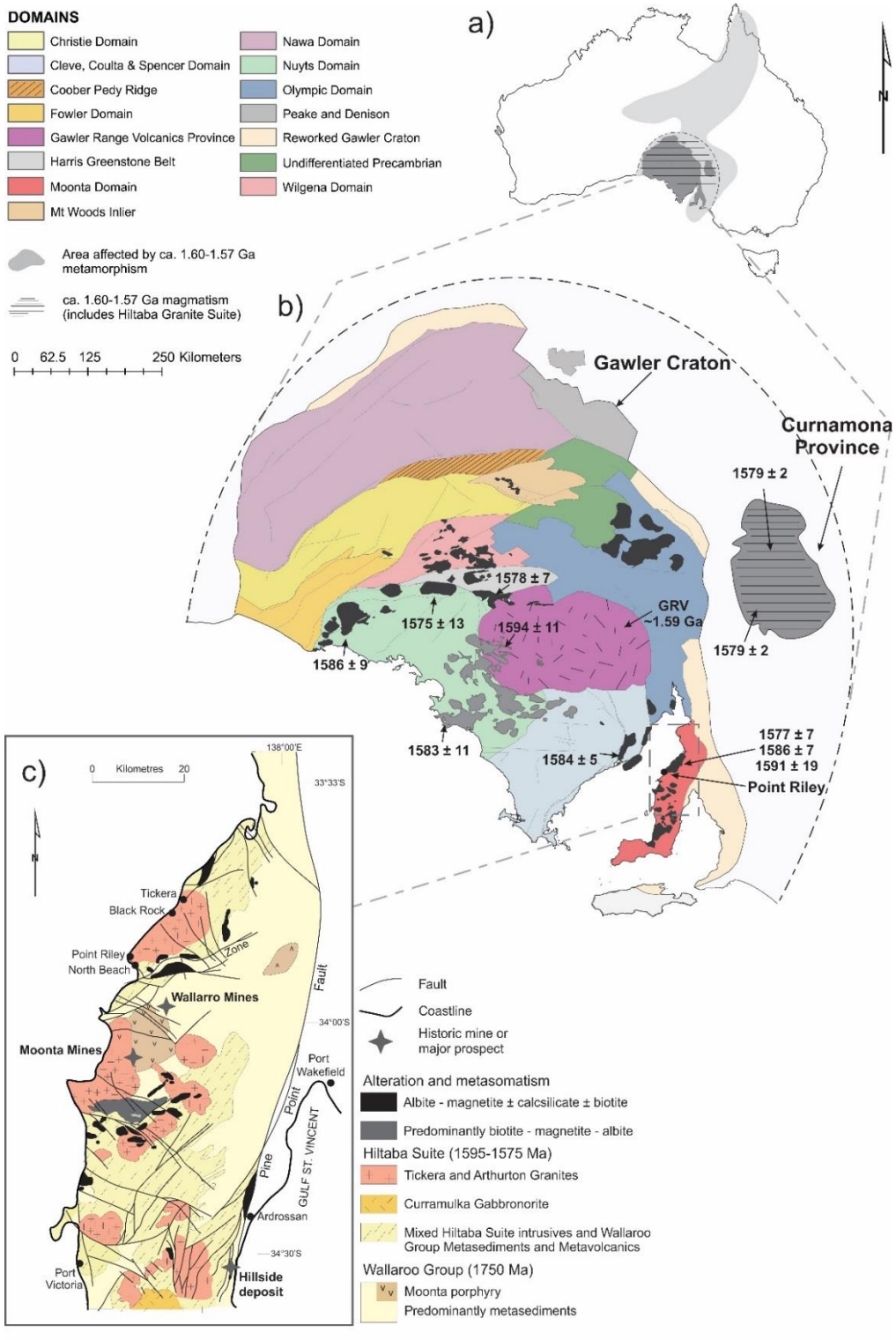


**Figure 1. (a) Map of Australia showing the area of Proterozoic Australia affected by tectonothermal activity and magmatism during the ca. 1600–1580 Ma time slice; (b) Simplified geological map of the Gawler Craton showing the distribution of Hiltaba Suite plutons, the Gawler Range Volcanics and geological domains after Stewart & Foden (2003); (c) Solid geology map of the Yorke Peninsula displaying the distributions of the Arthurton and Tickera Granites, modified after Conor et al., (2010). Mapping and sample locations of Point Riley, and sample locations of Black Rock and Wallaroo North Beach are shown.**

Paleoproterozoic, forming the Sleaford Complex and Mulgathing Complex in the in the southern and central western Gawler Craton respectively. The Gawler Craton was deformed and metamorphosed during the ca. 2480–2420 Ma Sleafordian Orogeny (Daly & Fanning 1993; Daly et al., 1998; Reid & Hand 2012). Recurrence of magmatism in the southeastern Gawler Craton at 2000 Ma lead to the development of the Miltalie Gneiss (Daly et al., 1998; Fanning et al., 1998, 2007).

Onset of basin formation resulted in deposition of the Hutchison Group at ca. 2000–1730 Ma (Parker et al. 1988; Hand et al., 2007). Basin development was interrupted at ca. 1850 Ma with emplacement of the Donington Suite along the eastern margin of the Gawler Craton during compressional deformation associated with the Cornian Orogeny (Reid et al., 2008). Subsequent emplacement of bimodal packages included the Broadview Schist and Myola Volcanics (ca. 1791 Ma: Parker et al., 1993; Fanning et al., 1988), and McGregor Volcanics (1740 Ma: Fanning et al., 1988). Sedimentary packages were also emplaced during this time interval and include the Price Metasediments (ca. 1767 Ma: Oliver and Fanning et al., 1997), Moonabie Formation (ca. 1756 Ma: Jagodzinski., 2005), the Wallaroo Group (1760–1740 Ma: Cowley et al., 2003), and unnamed sediments in the Nawa and Fowler Domains (Parker et al., 1993; Daly et al., 1998; Hand et al., 2007).

The Gawler Craton underwent a second tectonothermal event during the ca. 1730–1690 Ma Kimban Orogeny (Hoek & Schaefer 1998; Ferris et al. 2002; Hand et al. 2007). Intrusive rocks associated with the Kimban Orogeny include the ca. 1745–1700 Ma Peter Pan Supersuite (e.g. Wade & McAvaney 2016). Sedimentary packages include the ca. 1715 Ma Eba and Labrinyth Formations (Cowley and Martin 1991; Fanning et al., 2007). The Kimban Orogeny was followed by intrusion of the 1660–1640 Ma Tunkillia

Suite (Teasdale 1997; Daly et al. 1998; Ferris et al. 2002), and later eruption of the 1630 Ma Nuyts Volcanics (Rankin et al., 1990).

The St. Peter Suite intruded at ca. 1640–1608 Ma (Teasedale 1997; Daly et al. 1998; Swain et al., 2008; Symington et al., 2014). Bimodal volcanism that resulted in the emplacement of the Gawler Range Volcanics and Hiltaba Suite occurred between 1595–1575 Ma and was synchronous with regional deformation (e.g. Flint et al., 1993; Conor 1995; Creaser & Cooper 1993; Fanning et al., 2007). The Hiltaba Suite is suggested to have been generated from mafic underplating associated with lithospheric attenuation, and melting of the overlying continental crust (Flint et al., 1993; Zang et al., 2007). Geochemical variations within the Hiltaba Suite granites across the Gawler Craton is suggested to be due to their derivation from a depleted mantle source that mixed with various crustal components (Stewart & Foden 2003). Further deformation across the Gawler Craton occurred during the ca. 1570–1540 Ma Kararan Orogeny and ca. 1470–1450 Coorabie Orogeny (Hand et al., 2007).

## REGIONAL GEOLOGY OF THE YORKE PENINSULA

The Yorke Peninsula is part of the Moonta Domain in the southeastern Gawler Craton, South Australia (Fig. 1b,c). The area comprises late Paleoproterozoic metasediments and metavolcanics of the ca. 1750 Ma Wallaroo Group (Cowley et al., 2003), which extends northward from Yorke Peninsula, below the Stuart Shelf and along much of the Olympic Domain (Fig. 1b; Conor et al., 2010). Fine-grained psammites, siltstones, calcsilicates, albitites, quartzites and iron rich sediments of the Wandearah Formation dominate the Wallaroo Group (Conor 1995; Cowley et al., 2003). These metasediments were contemporaneously deposited with bimodal A-type volcanics of the Weetula Formation and Matta Formation (Cowley et al., 2003).

The Wallaroo Group preserves evidence of metamorphism and multiple folding events (e.g. Conor et al., 2010). Metamorphic grade varies from upper greenschist in the northern Yorke Peninsula to amphibolite facies in south (Conor et al., 2010). Two phases of deformation are preserved in the Wallaroo Group metasediments. The first phase involved generation of isoclinal folds with limbs extending up to several kilometres in length. The timing of this deformation event is suggested to be related to the ca. 1730–1690 Ma Kimban Orogeny, however this is equivocal (e.g. Conor et al. 2010). The second deformation phase involved refolding of the isoclinal folds by open upright folds (Conor 1995; Conor et al., 2010). Late folding is suggested to be associated with deformation during ca. 1600–1570 Ma time period based on preservation of amphibolite-rich calcsilicate alteration within the axial plane of the open upright folds, and that is interpreted to be related to alteration associated with intrusion of the Hiltaba Suite granites (Conor et al., 2010).

Within the Yorke Peninsula, the mafic component of the Hiltaba Suite is recognised as the Curramulka Gabbronorite, which facilitated melting of the lower crust to form its felsic component, the Arthurton and Tickera granites (Zang et al., 2007). The Tickera Granite, located in the northern Yorke Peninsula (Fig. 1c) preserves high strain deformation, which has been used to suggest that the granite was intruded into a tectonic regime in which shearing was prominent (Wurst 1994; Conor 1995). Conversely, the Arthurton Granite to the south is undeformed and suggested to postdate local deformation (Conor 1995; Conor et al., 2010).

## METHODS

Point Riley on the western Yorke Peninsula preserves a well–exposed shore platform of multiple phases of the Tickera Granite. The platform was mapped in detail to show the distribution and intrusive relationships of granite phases and preserved structural fabrics (Fig. 2).

Twelve samples were collected from Point Riley and are representative of the four granite phases that were identified during mapping. These samples were spatial distributed across the mapping area, were *in situ* and as fresh as possible. Two additional samples representing the southern and northern extent of the Tickera Granite were collected; 2.87 km south–east of Point Riley at Wallaroo North Beach (sample 2149822) and 7.87 km northeast of Point Riley at Black Rock (sample 2149823). Sample locations are shown in Figure 2. The samples were used for a combination of petrography, whole rock geochemistry and Sm–Nd isotopic analysis (Table 1).

Twelve samples were used for whole rock geochemical analysis (Table 1). All samples were prepared using a rock saw at the University of Adelaide. Crushing and whole rock geochemical analysis was undertaken at Australian Laboratory Services Pty. Ltd. using standard preparation methods (e.g. crushing and pulverising). Major and trace elements were analysed by inductively coupled plasma mass spectrometry (ICP–MS).

Eight samples were analysed for Sm–Nd isotope geochemistry: six from Point Riley, one from North Beach and one from Black Rock (Table 1). Samples from Point Riley were selected to represent each of the granite phases observed and based on their spatial distribution and trace element and rare earth element geochemistry, particularly their Sm and Nd content. Samples collected from Wallaroo North Beach and Black Rock were analysed to provide a broader understanding of the Sm–Nd isotopic composition

of the Tickera Granite across the northern Yorke Peninsula. Sm–Nd analysis was undertaken following the method of Wade et al. (2006) using a Finnigan MAT262 and MAT261 thermal ionisation mass spectrometer. $^{146}Nd/^{144}Nd$ ratio was normalised to 0.721903, Nd blanks corrected for 200 pg and Sm for 150 pg.

Eight samples were selected for petrographic analysis (Table 1). Samples included the six samples used for Sm–Nd analysis. Samples were prepared using a rock saw at the University of Adelaide and prepared by Thin Section Australia. Petrographic analysis was undertaken using standard transmitted and reflected light microscopy to assess mineralogy and textural relationships.

**Table 1. Analyses performed on samples collected from Point Riley, Black Rock and Wallaroo North Beach in this study.**

| Sample | Rock Type | Geochemistry | Petrography | Sm–Nd |
|---|---|---|---|---|
| **2147273** | Nodule | ✓ | ✓ | ✓ |
| **2147279** | Nodule | ✓ | | |
| **2147276** | Orange | ✓ | ✓ | ✓ |
| **2147280** | Orange | ✓ | | |
| **2147281** | Orange | ✓ | ✓ | ✓ |
| **2147272** | White | ✓ | ✓ | ✓ |
| **2147275** | White | ✓ | | |
| **2147277** | White | ✓ | ✓ | ✓ |
| **2147271** | Red | ✓ | | |
| **2147274** | Red | ✓ | | |
| **2147278** | Red | ✓ | | |
| **2147282** | Red | ✓ | ✓ | ✓ |
| **2149823** | Black Rock (Red) | | ✓ | ✓ |
| **2149822** | North Beach (Red) | | ✓ | ✓ |

# OBSERVATIONS AND RESULTS

## Field Observations

The Point Riley area (Figs. 1b, c and 2) preserves well exposed shore platforms of the Tickera Granite. Four phases of granite were recognised and are divided based on grain size, mineralogy, composition and deformation style. The four phases were granite nodules, an intensely foliated orange granite, a white leucogranite and a red granite.

### Granite nodules

Granite nodules are preserved throughout the intensely foliated orange granite (Figs. 2 and 3a). The nodules extrude from the surrounding foliated granite, are up to 30 cm length and oval in shape. The nodules comprise medium grained K–feldspar (60%; 1–5 mm), quartz (30%; 1–4 mm) and amphibole (10%; 2 mm) (Fig. 3a). Mineral grains vary from rounded (K–feldspar and quartz) to sub–rounded (amphibole) and elongated within a well–developed, northeast–trending foliation that dips steeply to the northwest. This foliation is also preserved in the surrounding foliated orange granite.

### Intensely foliated orange granite

The dominant phase in the mapping area is an intensely foliated orange granite that is recessively weathered (Figs. 2 and 3a–c). The foliated orange granite shares similar mineralogy to the granite nodules. Mineral grains are sub–rounded to rounded, vary in size from medium– to coarse–grained and comprise K–feldspar (70%; 1–8 mm), quartz (~15%; 1–4 mm), biotite and amphibole (10% mafics; 1–2 mm), and small quantities of plagioclase (<5%; 1 mm). Hematite alteration is evident in this phase through its red/orange colour.

The orange granite preserves a well–developed, pervasive foliation (Figs. 2, 3a–c and 4a) defined by K–feldspar and quartz crystals. The foliation is northeast–trending and steeply northwest or southeast dipping. A locally well–developed cleavage is also preserved in the orange foliated granite, particularly in areas close to the contact boundaries with the red and white granite phases within which the cleavage is a dominant feature. The cleavage is discontinuous, northwest–trending and moderately to steeply northeast dipping.

Enclaves of undeformed orange granite are locally preserved within the intensely foliated orange granite in the northwestern part of the study area (Fig. 2). Metasedimentary xenoliths of the Wallaroo Group are also preserved within the same local area and range in size from 20cm–1m and comprise fine–grained metapelites (Fig. 2). Quartz and K–feldspar veins which are 5–30 cm thick cross–cut this phase throughout the study area.

White leucogranite

A white leucogranite forms prominent, blocky exposures throughout the study area (Figs. 2 and 3d–f). The leucogranite is medium– to coarse–grained and comprises plagioclase (60%; 1–3 mm), quartz (~35%; 1–2 mm) and minor mafics (<5%; 1 mm). All grains are sub–rounded.

Two distinct cleavages are evident in the white leucogranite (Figs. 2, 3d, f and 4b). The first is a locally well–developed, 5–30 cm spaced, northeast–trending and moderately to steeply northwest dipping cleavage. The second cleavage is a moderate to well–developed northwest–trending cleavage and dips steeply to the northeast. This cleavage is 10–100 cm spaced and is evident throughout the whole mapping area. A poorly

developed mineral lineation is locally preserved and is defined by the alignment of quartz and feldspar crystals.

Red granite

A deformed red granite intrudes through all phases as a sheeted dyke and outcrops at both high and low reliefs across the study area (Figs. 2 and 3b, e–g). The red granite comprises coarse, sub–rounded grains of K–feldspar (55%; 1–5 mm), quartz (35%; 1–3 mm) and minor amounts of amphibole (10%; 1–2 mm). Within the high relief outcrops of the red granite, cavities ranging in size from 3–5 mm are preserved (Figs. 2 and 3g). Hematite alteration is also evident by the red colouration of the granite.

A well–developed foliation is locally preserved along the margins of the red granite dyke within 50cm of the contact boundary with the intensely foliated orange granite (Figs. 2, 3b and 4c). The foliation is defined by elongate quartz and K–feldspar crystals, is northeast–trending and steeply dips to the northwest. A well–developed, 5–30 cm spaced, northwest–trending, moderately to steeply northeast or southwest dipping cleavage is locally preserved (Figs. 2 and 4c). This cleavage is continuous into the other granite phases.

Contact relationships

The contact boundaries between the foliated orange granite, white leucogranite and red granite are sharp in most cases (Figs. 3b, c, f). The white leucogranite locally intrudes the foliated orange granite as metre–scale fingers along the foliation plane of the enclosing orange granite phase. The fingers are 20–30 cm wide and up to 3m in length (Fig. 2). In the centre of the map area, small 5–10cm long apophyses of the white leucogranite observed intruding into the foliated orange granite (Figs. 2 and 3c).

Evidence of contact metamorphism between the red granite and white leucogranite is locally preserved (Figs. 2 and 3e). The contact metamorphic boundary ranges in thickness from 5–20 cm, and is manifest by a colour difference between the two phases, where the white leucogranite gradually becomes redder in colour. Approximately 2 m east of the contact metamorphic boundary, a raft of white leucogranite is preserved within the red granite dyke, which itself is surrounded by the white leucogranite (Figs. 2 and 3f). The white leucogranite raft is rounded, approximately 1x2 m size. In the northeastern section of the study area, evidence of magma mingling between the red granite dyke and white leucogranite is evident (Figs. 2 and 3h); contact boundaries are highly irregular and often unclear. Mixing appears to be incomplete. Iron staining on the surface of the white leucogranite is also a prominent feature in this part of the study area.

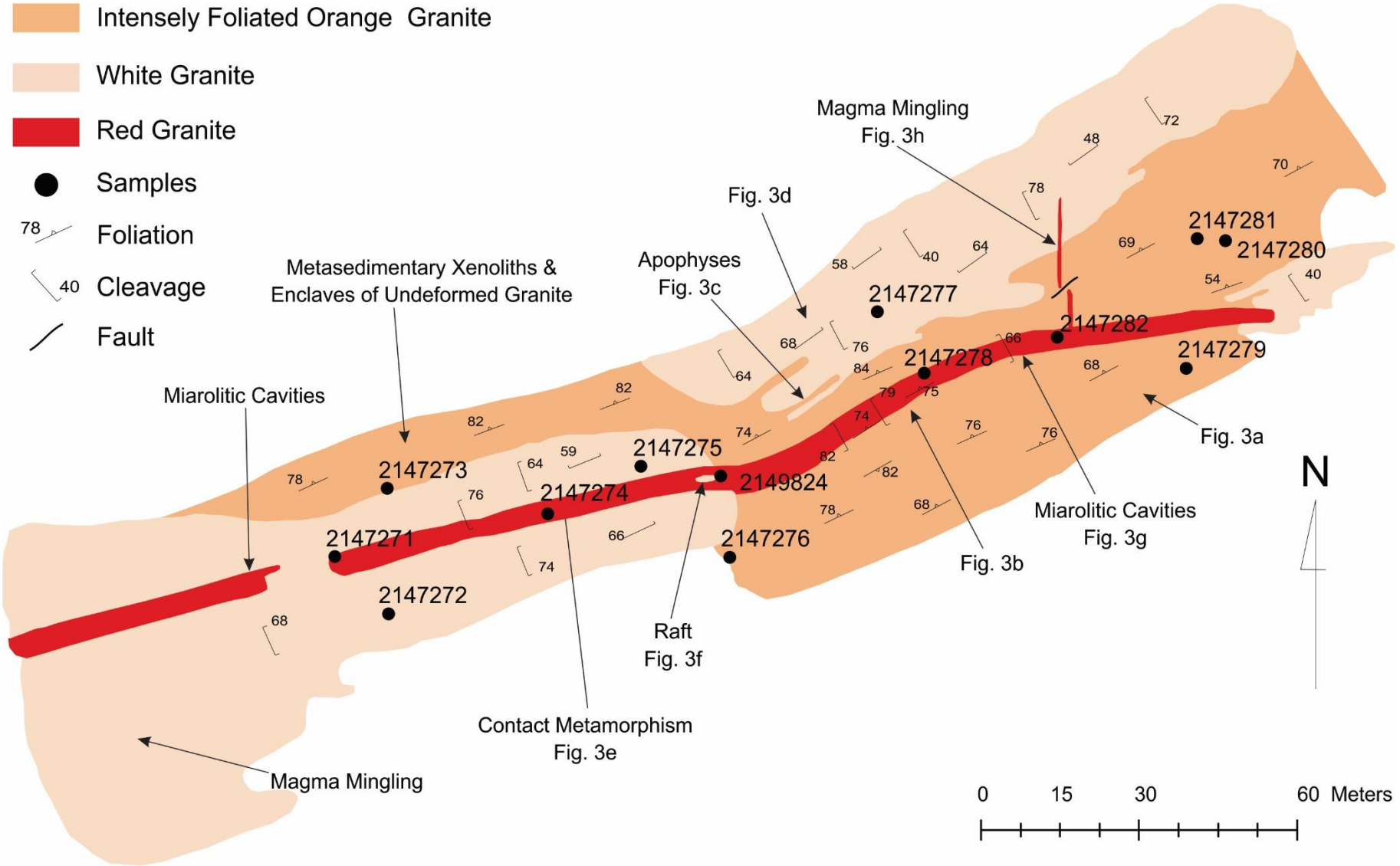


**Figure 2. Geological surface map of Point Riley showing the mapped phases of the Tickera Granite, sample locations, structures observed and intrusive magmatic features. Map location shown in Figure 1c.**

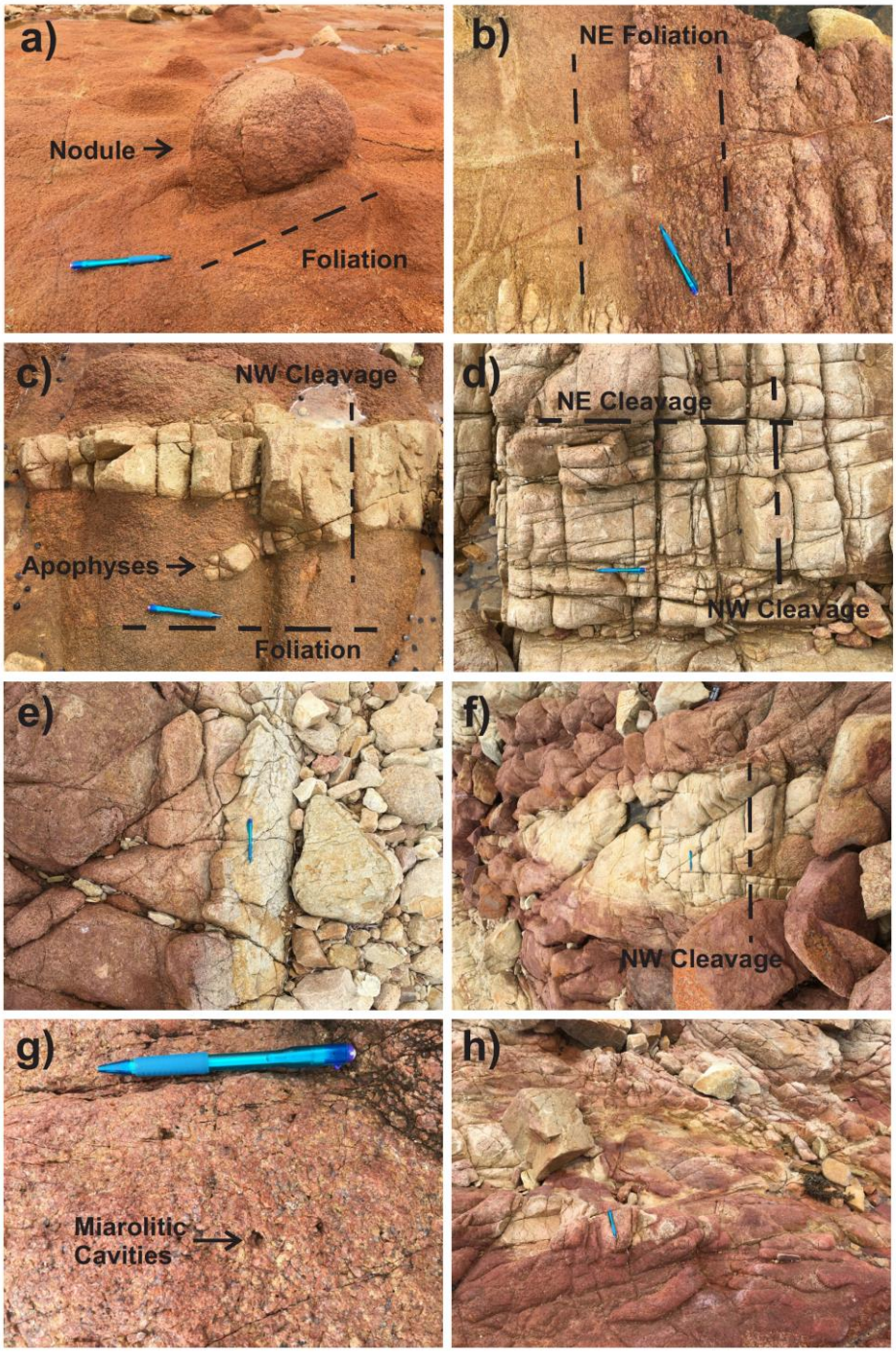


**Figure 3. Representative photos of granite phases and contact relationships observed at Point Riley. (a) Granitic nodule within the intensely foliated orange granite. The recessive nature and the intense NE–trending foliation can be seen in the orange granite. Photo taken looking north; (b) Contact boundary between foliated orange granite (left) and red granite (right) showing the well–developed NE–trending foliation preserved within both granite phases. Photo taken looking southwest; (c) White leucogranite apophyses intruding into the surrounding foliated orange granite; (d) Two cleavages in the white leucogranite. Photo taken looking northwest; (e) Contact metamorphic boundary between the white and red granites. Northeast to the top of photo; (f) Raft of white leucogranite within the red granite dyke. Photo taken looking northwest; (g) Miarolitic cavities in the red granite. Photo taken looking southeast; (h) Magma mingling between the white and red granite phases. Photo taken looking east. Location of photos shown in Figure 2.**

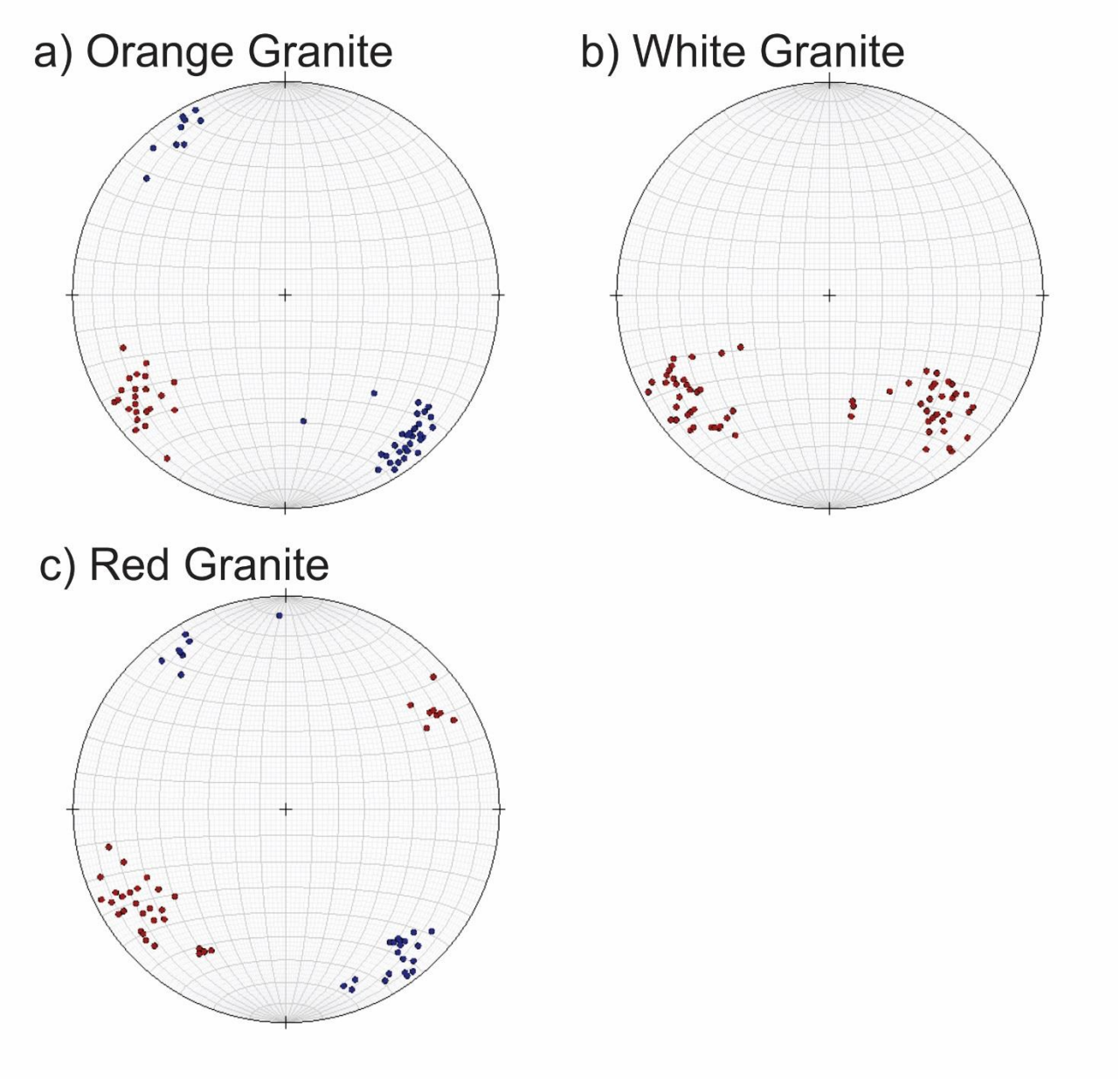


**Figure 4. Stereonet plots showing foliation (blue) and cleavage (red) data plotted as poles to planes for the (a) orange, (b) white and (c) red granite phases.**

## Petrography

Granite nodules

The granite nodules primarily comprises microcrystalline K–feldspar, quartz, magnetite, biotite and plagioclase. Few K–Feldspars are microcline, and the majority show evidence of significant sericite alteration and hematite staining. Biotite is subhedral while magnetite is euhedral, and are both fine grained and randomly distributed throughout the granite. Hematite–filled veins also cross cut all minerals (Fig. 5a).

Intensely foliated orange granite

The orange granite comprises K–feldspar, quartz, biotite, magnetite, plagioclase and minor amphibole. Few K–Feldspars are microcline, and the majority show evidence of significant sericite alteration and hematite staining. Vermicelli type exsolution is commonly observed within feldspars. Biotite is euhedral and along with K-feldspar is aligned within the dominant foliation preserved in the granite. Localised brecciation shows a stockwork of hematite veining that is predominantly developed around altered feldspars and within quartz grains (Fig. 5b).

White leucogranite

The white leucogranite dominantly comprises plagioclase and quartz, with minor magnetite. Plagioclase is significantly sericite altered. Thin hematite veins occasionally cross cut quartz and plagioclase (Fig. 5c).

Red granite

The red granite generally comprises medium to coarse grained K–feldspar and quartz, with minor plagioclase, magnetite and biotite. Minor microcline is observed. Sericite and hematite alteration of feldspars is preserved (Fig. 5d). Minor perthitic exolutions are also observed. At North Beach, a prominent foliation defined by quartz and

significantly sericite altered and brecciated feldspars, is locally preserved within the red granite (Fig. 5e). At Black Rock, the red granite also contains amphibole, with higher modal proportion of biotite and more intense sericite alteration (Fig. 5f). Minor hematite is commonly preserved and is present in thin veins.

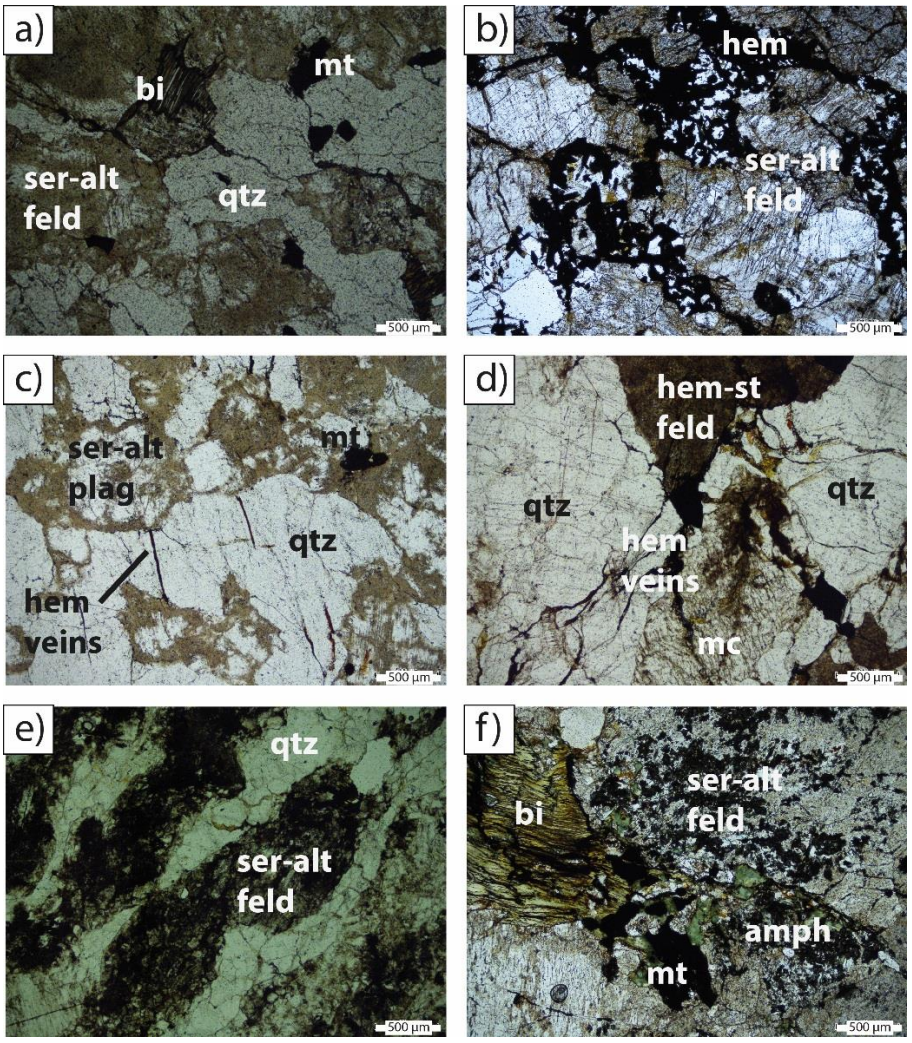


**Figure** 5**. Representative plane polarised photomicrographs of Tickera Granite phases at Point Riley. (a) Granitic nodule illustrating sericitised feldspar, with biotite and magnetite localised around the edges; (b) Orange granite displaying a stockwork of hematite filled veins and altered feldspar. Sample 2147281; (c) White granite displaying sericitised plagioclase, quartz, minor magnetite and thin hematite filled veins. Sample 2147277; (d) Red granite displaying hematite stained feldspar, quartz, hematite veins and microcline; (e) North Beach red granite (2149822) displaying foliation defined by brecciated, altered feldspars and quartz; (f) Black Rock red granite (2149823) displaying abundance of biotite and amphibole, sericitised feldspars and minor magnetite. Mineral abbreviations: ser-alt feld: sericite-altered feldspar; bi: biotite; mt: magnetite; hem: hematite; ser-alt plag: sericite-altered plagioclase; qtz: quartz; mc: microcline; amph: amphibole**

## Geochemistry

### Major Elements

Major element geochemical results for the nodules, orange, white and red granites are displayed in Figure 6 and Table 2. The $SiO_2$ content of the Tickera Granite ranges from 69.9–79.2 wt%. The orange foliated granite has $SiO_2$ content of 69.9–71.1 wt%, the nodules range from 71.1–73.4 wt%, whilst the white leucogranite clusters around 77 wt%. The red granite shows the widest variation in $SiO_2$ content of 70–79 wt% (Fig. 6). $Al_2O_3$, $P_2O_5$, MgO and $TiO_2$ display a negative trend with increasing $SiO_2$ content for all samples (Fig. 6a–d). $Fe_2O_3$ content has a steep negative correlation for $SiO_2$ content between 69.9–~72 wt%, which then becomes shallower with higher $SiO_2$ content (Fig. 6e). A negative trend is observed for CaO and $Na_2O$ with increasing $SiO_2$ in the foliated orange granite, nodules and red granite phases (Fig. 6f–g). The white leucogranite however, has a relatively high CaO and $Na_2O$ content compared to other phases (Fig. 6f–g). $K_2O$ is scattered; the white leucogranite phase shows relatively low $K_2O$ contents (Fig. 6h). MnO content for most samples are below detection limit except for two of the lower silica phase samples (2147271 and 2147280; Table 2, Fig. 6i). The white leucogranite is rich in CaO and $Na_2O$, and depleted in $K_2O$, reflecting the high albite content (Fig. 6j–k). The red granite is rich in $K_2O$ and depleted in CaO and $Na_2O$, reflecting the high K–feldspar content (Fig. 6j–k). The orange granite and nodules are intermediate between the two and each have an outlier (Fig. 6j–k).

**Table 2**. Major and trace element geochemical data for samples from Point Riley. Sample location shown in Figure 2.

| Sample | Unit | 2147276 | 2147280 | 2147281 | 2147273 | 2147279 | 2147272 | 2147275 | 2147277 | 2147271 | 2147274 | 2147278 | 2147282 |
|---|---|---|---|---|---|---|---|---|---|---|---|---|---|
| Description | | Orange granite | Orange Granite | Orange Granite | Nodule | Nodule | White Granite | White Granite | White Granite | Red Granite | Red Granite | Red granite | Red Granite |
| $SiO_2$ | % | 69.90 | 70.80 | 71.10 | 73.40 | 71.10 | 76.80 | 76.90 | 76.70 | 70.40 | 74.00 | 79.20 | 76.00 |
| $TiO_2$ | % | 0.47 | 0.48 | 0.11 | 0.23 | 0.43 | 0.17 | 0.23 | 0.23 | 0.54 | 0.18 | 0.23 | 0.14 |
| $Al_2O_3$ | % | 14.00 | 14.35 | 14.95 | 13.60 | 14.20 | 13.50 | 14.00 | 14.00 | 11.95 | 12.90 | 11.70 | 12.50 |
| $Fe_2O_3$ | % | 4.19 | 4.69 | 2.40 | 2.67 | 3.73 | 0.96 | 0.93 | 1.06 | 6.42 | 1.87 | 1.96 | 2.06 |
| MnO | % | 0.01 | 0.02 | 0.01 | 0.01 | 0.01 | 0.01 | 0.01 | 0.01 | 0.02 | 0.01 | 0.01 | 0.01 |
| MgO | % | 0.58 | 0.51 | 0.34 | 0.17 | 0.16 | 0.05 | 0.09 | 0.06 | 0.21 | 0.07 | 0.09 | 0.13 |
| CaO | % | 0.57 | 0.85 | 0.08 | 0.55 | 0.93 | 1.62 | 1.08 | 1.04 | 0.36 | 0.28 | 0.33 | 0.26 |
| $Na_2O$ | % | 4.03 | 4.11 | 3.97 | 4.04 | 5.52 | 5.20 | 5.57 | 5.57 | 3.17 | 2.94 | 2.93 | 2.71 |
| $K_2O$ | % | 4.26 | 3.80 | 6.83 | 4.30 | 1.31 | 1.22 | 1.24 | 1.43 | 5.01 | 5.86 | 4.87 | 6.06 |
| $P_2O_5$ | % | 0.03 | 0.05 | 0.01 | 0.06 | 0.09 | 0.02 | 0.01 | 0.01 | 0.08 | 0.02 | 0.02 | 0.01 |
| LOI | % | 1.17 | 1.25 | 0.96 | 0.61 | 0.98 | 0.43 | 0.59 | 0.54 | 0.65 | 0.53 | 0.41 | 0.46 |
| Total | % | 99.21 | 100.91 | 100.76 | 99.64 | 98.46 | 99.98 | 100.65 | 100.65 | 98.81 | 98.66 | 101.75 | 100.34 |
| F | ppm | 590.00 | | | | 470.00 | | 130.00 | | | | 110.00 | |
| Rb | ppm | 420.00 | 329.00 | 383.00 | 222.00 | 105.00 | 60.50 | 67.20 | 72.10 | 270.00 | 355.00 | 303.00 | 374.00 |
| Sr | ppm | 152.00 | 181.50 | 35.70 | 251.00 | 400.00 | 144.00 | 119.00 | 113.00 | 306.00 | 84.50 | 83.80 | 83.90 |
| Cs | ppm | 2.55 | 2.26 | 0.81 | 1.38 | 1.73 | 0.56 | 1.02 | 1.12 | 0.78 | 0.94 | 0.96 | 0.84 |
| Ba | ppm | 668.00 | 683.00 | 758.00 | 712.00 | 177.00 | 74.40 | 75.40 | 122.00 | 1140.00 | 597.00 | 527.00 | 609.00 |
| Th | ppm | 25.70 | 65.30 | 27.20 | 122.00 | 49.80 | 90.90 | 115.50 | 65.80 | 37.60 | 121.50 | 104.50 | 98.60 |
| U | ppm | 6.31 | 8.49 | 1.81 | 13.45 | 5.50 | 3.74 | 2.52 | 2.77 | 6.59 | 8.66 | 6.66 | 3.65 |
| Pb | ppm | 6.00 | 5.00 | 3.00 | 17.00 | 38.00 | 12.00 | 5.00 | 3.00 | 9.00 | 5.00 | 2.00 | 9.00 |
| Nd | ppm | 16.80 | 24.80 | 2.40 | 59.00 | 44.10 | 20.00 | 14.60 | 4.50 | 25.50 | 24.20 | 22.20 | 13.40 |
| Ta | ppm | 2.60 | 2.70 | 1.80 | 5.00 | 2.70 | 2.90 | 3.80 | 3.90 | 3.30 | 4.10 | 6.50 | 3.30 |
| Zr | ppm | 319.00 | 313.00 | 149.00 | 277.00 | 305.00 | 212.00 | 271.00 | 261.00 | 708.00 | 103.00 | 42.00 | 61.00 |
| Hf | ppm | 8.00 | 8.00 | 4.50 | 7.90 | 7.70 | 6.10 | 7.80 | 7.70 | 17.40 | 2.90 | 1.40 | 2.00 |
| Y | ppm | 12.00 | 14.20 | 6.70 | 49.20 | 21.60 | 9.80 | 12.70 | 8.70 | 18.00 | 62.90 | 16.30 | 11.40 |
| Sc | ppm | 6.00 | 5.00 | 1.00 | 4.00 | 5.00 | 1.00 | 1.00 | 1.00 | 7.00 | 5.00 | 3.00 | 4.00 |
| V | ppm | 40.00 | 41.00 | 30.00 | 27.00 | 48.00 | <5 | <5 | <5 | 26.00 | <5 | 6.00 | 13.00 |
| Cr | ppm | 20.00 | 20.00 | 10.00 | 10.00 | 10.00 | <10 | <10 | 10.00 | 10.00 | 10.00 | <10 | 10.00 |
| Co | ppm | 4.00 | 7.00 | 1.00 | 2.00 | 2.00 | 2.00 | 1.00 | 2.00 | 3.00 | 1.00 | <1 | 2.00 |
| Ni | ppm | 1.00 | 2.00 | 2.00 | 2.00 | 1.00 | 1.00 | 3.00 | <1 | 3.00 | 2.00 | 2.00 | <1 |
| Cu | ppm | 8.00 | 27.00 | 2.00 | 5.00 | 4.00 | 3.00 | 5.00 | 2.00 | 4.00 | 6.00 | 3.00 | 4.00 |
| Zn | ppm | 7.00 | 7.00 | 2.00 | 6.00 | 5.00 | 4.00 | 5.00 | 5.00 | 8.00 | 7.00 | 5.00 | 5.00 |
| Ga | ppm | 22.50 | 21.70 | 22.00 | 19.80 | 23.80 | 19.50 | 19.90 | 20.30 | 18.90 | 18.10 | 17.40 | 17.20 |
| Ag | ppm | <0.5 | <0.5 | <0.5 | <0.5 | <0.5 | <0.5 | <0.5 | <0.5 | <0.5 | <0.5 | <0.5 | <0.5 |
| Sn | ppm | 6.00 | 5.00 | 3.00 | 5.00 | 8.00 | 4.00 | 6.00 | 6.00 | 9.00 | 4.00 | 5.00 | 3.00 |
| La | ppm | 16.70 | 39.00 | 4.00 | 47.50 | 65.80 | 10.10 | 6.20 | 3.40 | 51.40 | 29.70 | 31.30 | 18.50 |
| Ce | ppm | 41.00 | 77.10 | 7.60 | 111.00 | 126.00 | 27.20 | 18.10 | 5.90 | 98.30 | 60.50 | 69.00 | 39.60 |
| Pr | ppm | 4.83 | 8.29 | 0.70 | 15.65 | 13.85 | 5.08 | 3.52 | 1.12 | 8.65 | 7.08 | 7.15 | 4.30 |
| Nd | ppm | 16.80 | 24.80 | 2.40 | 59.00 | 44.10 | 20.00 | 14.60 | 4.50 | 25.50 | 24.20 | 22.20 | 13.40 |
| Sm | ppm | 3.48 | 4.37 | 0.52 | 13.35 | 8.20 | 4.32 | 3.28 | 1.16 | 4.13 | 5.73 | 3.74 | 2.34 |
| Eu | ppm | 0.71 | 0.65 | 0.20 | 2.05 | 1.41 | 0.91 | 0.79 | 0.47 | 0.87 | 0.99 | 0.54 | 0.56 |
| Gd | ppm | 2.47 | 2.74 | 0.62 | 10.10 | 5.13 | 2.78 | 2.41 | 1.08 | 2.77 | 6.45 | 2.50 | 1.59 |
| Tb | ppm | 0.37 | 0.39 | 0.13 | 1.42 | 0.70 | 0.38 | 0.36 | 0.20 | 0.42 | 1.13 | 0.43 | 0.27 |
| Dy | ppm | 2.32 | 2.53 | 0.89 | 8.64 | 4.27 | 2.01 | 2.39 | 1.43 | 2.97 | 8.18 | 2.99 | 1.98 |
| Ho | ppm | 0.43 | 0.50 | 0.22 | 1.65 | 0.79 | 0.36 | 0.48 | 0.32 | 0.64 | 1.86 | 0.61 | 0.39 |
| Er | ppm | 1.47 | 1.62 | 0.81 | 4.93 | 2.28 | 1.00 | 1.53 | 1.12 | 2.37 | 5.96 | 1.94 | 1.28 |
| Tm | ppm | 0.24 | 0.28 | 0.15 | 0.76 | 0.37 | 0.17 | 0.26 | 0.20 | 0.45 | 0.97 | 0.34 | 0.23 |
| Yb | ppm | 1.77 | 1.97 | 1.14 | 5.22 | 2.82 | 1.18 | 1.90 | 1.51 | 3.39 | 6.19 | 2.38 | 1.67 |
| Lu | ppm | 0.30 | 0.33 | 0.19 | 0.78 | 0.41 | 0.18 | 0.31 | 0.22 | 0.64 | 0.93 | 0.32 | 0.25 |
| Eu/Eu* | | 0.74 | 0.57 | 1.08 | 0.54 | 0.66 | 0.80 | 0.86 | 1.28 | 0.79 | 0.50 | 0.54 | 0.89 |
| $(La/Yb)_{Nb}$ | | 6.38 | 13.38 | 2.37 | 6.15 | 15.77 | 5.78 | 2.21 | 1.52 | 10.25 | 3.24 | 8.89 | 7.49 |

Eu/Eu* = (Eu/0.087)/(sqrt((Sm/0.231)*(Gd/0.306))) (Taylor & McLennan 1885)

REE Frac = $(La/Yb)_{Nb}$ = (La/0.367)/(Yb/0.248) (Taylor & McLennan 1985)

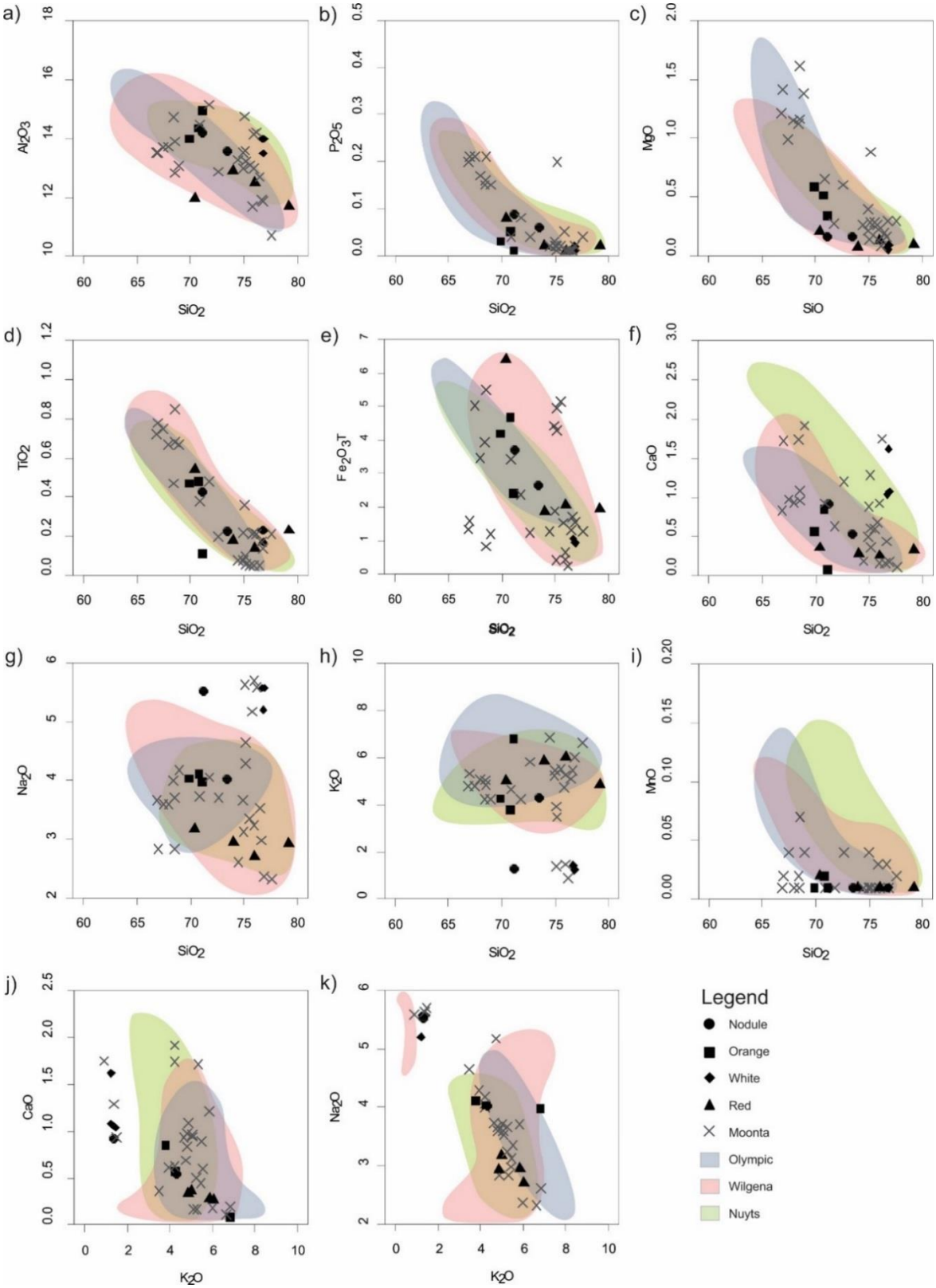


**Figure 6. Major element variation diagrams of major elements for samples from Point Riley. Sample location shown in Figure 2. Data from the Moonta (Creaser 1989; Wurst 1994; Giles 1980), Olympic (Creaser 1989; OZCHEM; SARIG), Wilgena (Foden & Stewart 2005; SARIG) and Nuyts (Foden & Stewart 2005; SARIG) domains are also shown for comparison.**

## Trace and Rare Earth Elements

Trace and rare earth element geochemical results are displayed in Figure 7 and Table 2. A positive correlation is evident in Th with increasing $SiO_2$ content whilst a negative trend is observed for Sc, Zr, Ba, Ce and La (Fig 7a–f). Sr has an overall negative trend although there is a slight inflection at ~73 wt% $SiO_2$ for Sr (Fig 7g).

Primitive mantle normalised multi element trace element plots show well defined patterns for each of the granite phases, and are characterised by positive anomalies in Rb, Th and Ta, and negative anomalies in Ba, Nb, P and Ti (Fig. 8). There is a slight variance in the Zr content where all but three red granite samples have a positive anomaly. (Fig. 8). Similarly, Pb shows a positive anomaly in all samples except one from each of the orange and red granite phases that have slight negative anomalies.

Chondrite normalised rare earth element (REE) diagrams are presented in Figure 9. All samples show moderately steep REE patterns due to relative enrichment in light REE (LREE), with moderate negative Eu anomalies (Eu/Eu* = 0.49–0.88) (Fig. 9 and Table 2). The nodules display the highest REE enrichment, followed by the red and orange granite, then the white granite (Fig. 9). One sample from the orange and white granite phases are relatively depleted in REE compared with other samples, have an overall flatter REE pattern and positive Eu anomalies (Eu/Eu* = 1.08 and 1.28). REE fractionation $(La/Yb)_{Nb}$ plotted against Eu/Eu* (Fig. 10) illustrates higher degrees of fractionation in the nodules, orange and red granite compared to the white leucogranite. The white leucogranite has consistently higher Eu values compared to the other granite phases, which preserve more variable Eu values.

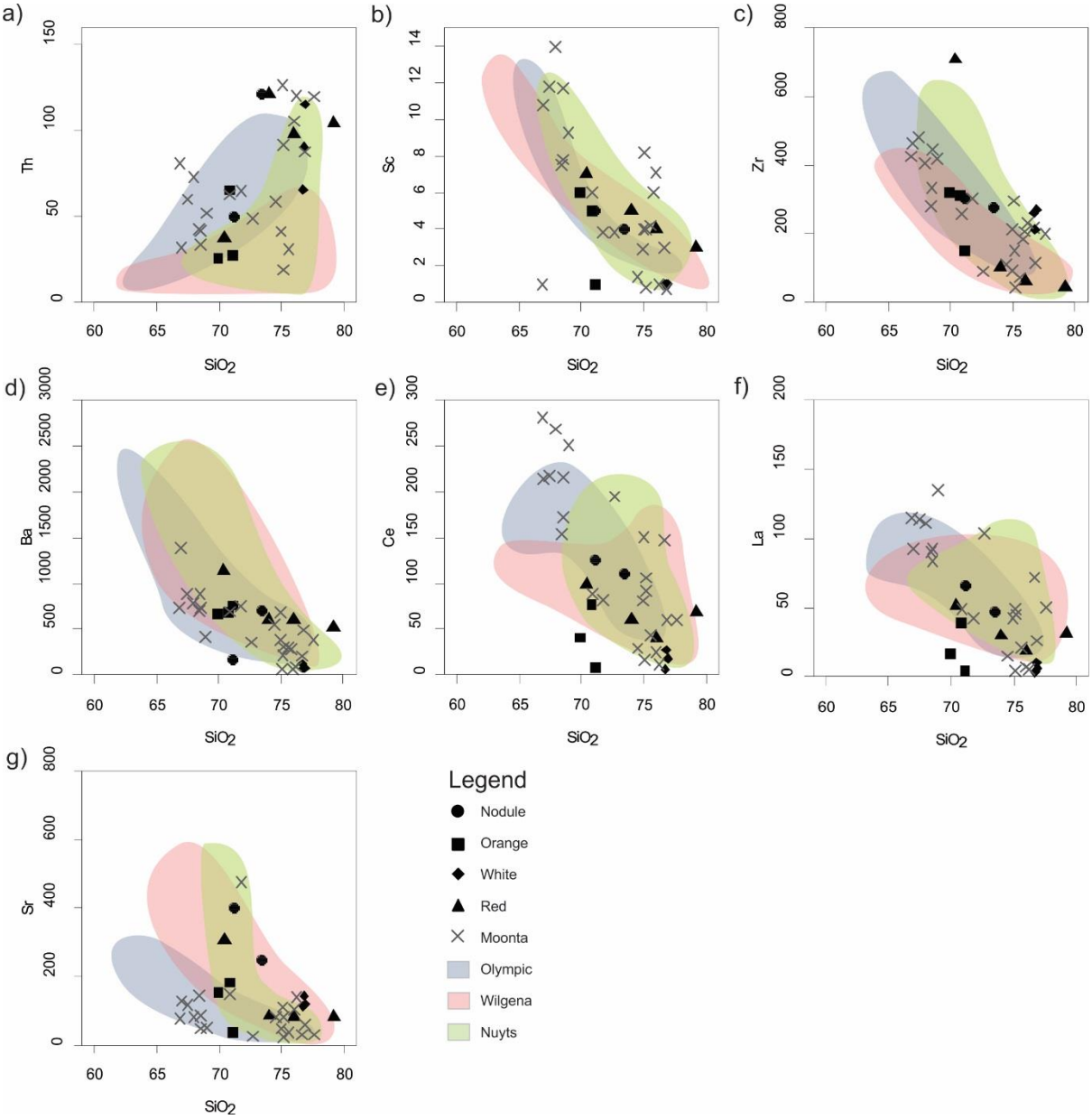


**Figure 7. Trace element variation diagrams of trace elements for samples from Point Riley. Sample locations shown in Figure 2. Data from the Moonta (Creaser 1989; Wurst 1994; Giles 1980), Olympic (Creaser 1989; OZCHEM; SARIG), Wilgena (Foden & Stewart 2005; SARIG) and Nuyts (Foden & Stewart 2005; SARIG) domains are also shown for comparison.**

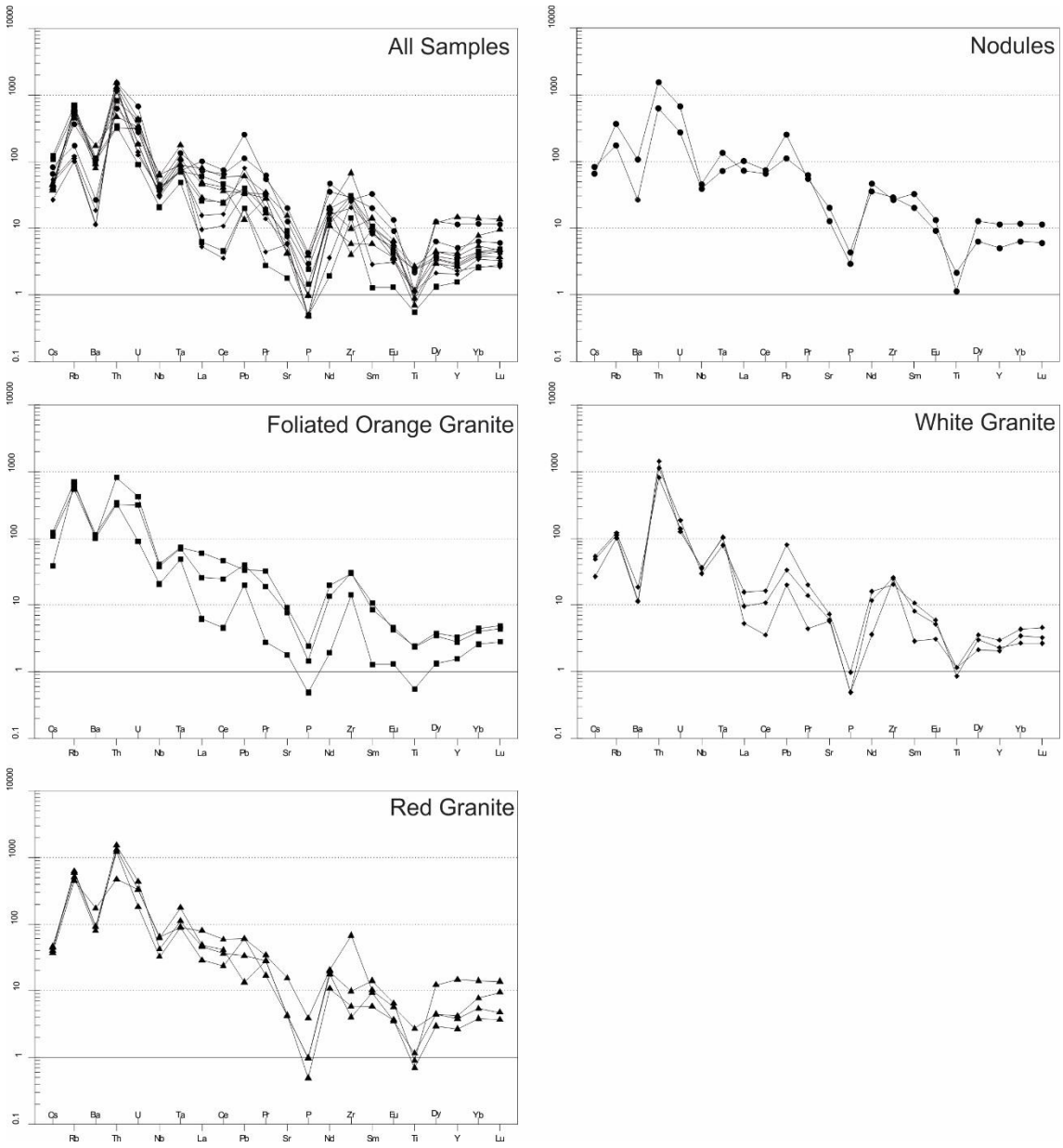


**Figure 8. Primitive mantle normalised trace element spidergrams for samples from Point Riley. Data normalised to values of McDonough & Sun (1995). Sample locations shown in Figure 2.**

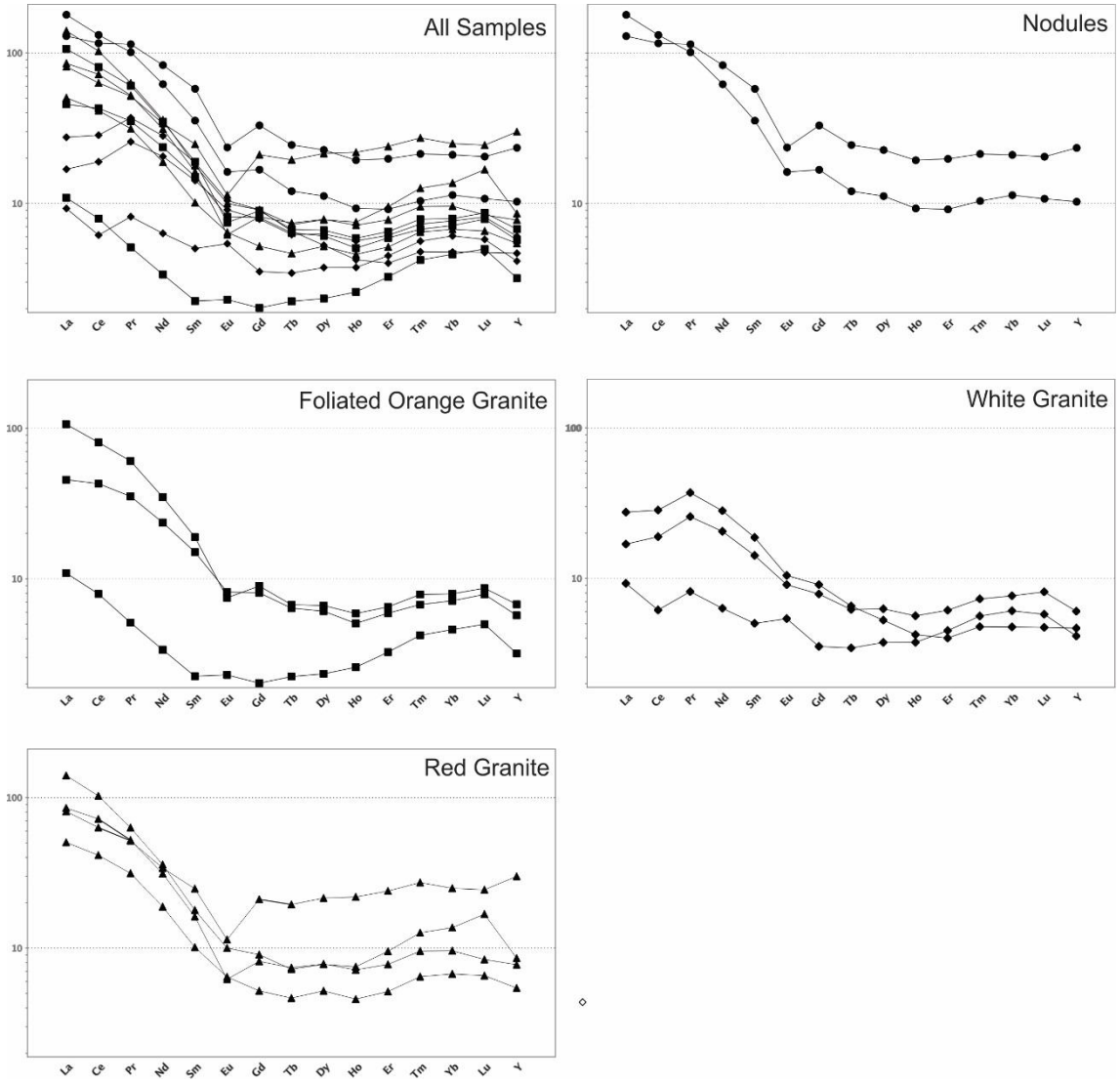


**Figure 9. Chondrite normalised REE spidergrams for Point Riley samples. Data normalised to values of Taylor & McLennan (1985). Sample locations shown in Figure 2.**

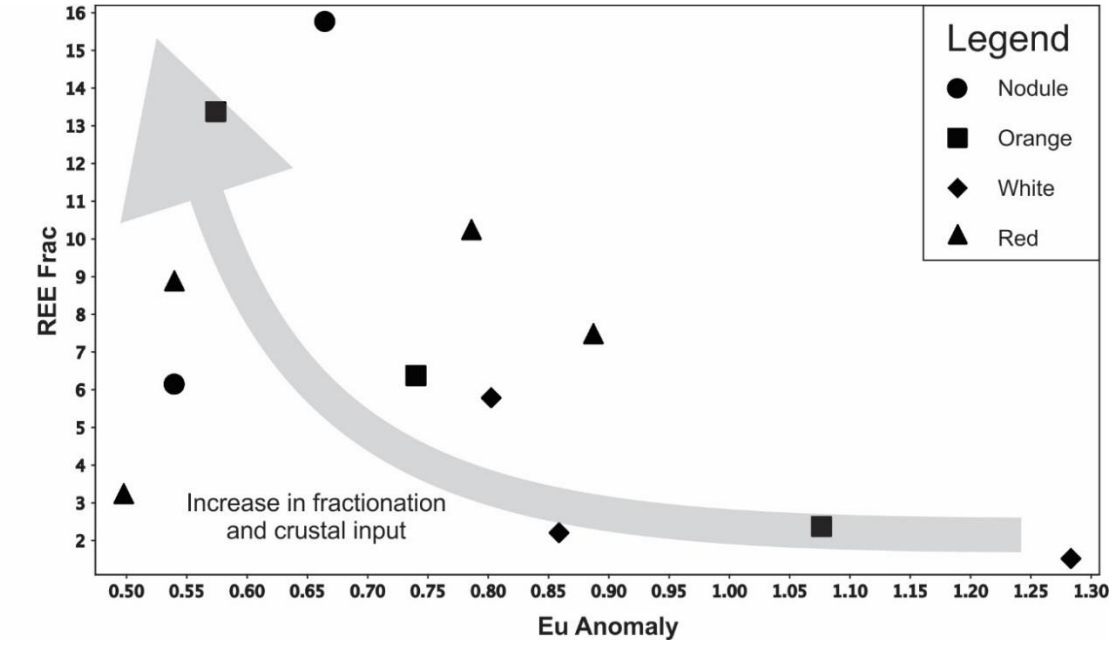


**Figure 10. Rare earth element fractionation (REE Frac) versus Eu anomaly plot for the Point Riley samples. Data normalised to Taylor & McLennan (1985). Equations used for calculations are given in Table 3. Sample location shown in Figure 2.**

## Sm–Nd isotope analysis

Sm–Nd isotope results for two intensely foliated orange granites, one nodule, two white and three red granite samples are given in Table 3 and Figure 11. Initial εNd(i) values were calculated at 1590, 1585 and 1580 for the orange, white and red granite phases respectively based on the known age of the Tickera Granite (ca. 1597–1577 Ma; Conor 1995) and interpreted relative timing of emplacement of the granite phases. εNd(i) values for the orange granite and nodule are well grouped and range from –6.73 and –3.55. The white and red granite phases have broad εNd(i) values ranging from –9.78 and –2.42 and –13.81 and –5.13 respectively. $^{147}Sm/^{144}Nd$ ratios range between 0.1294 and 0.1390 for the orange granite and nodules, 0.1296 and 0.1561 for the white leucogranite, and 0.1098 and 0.1663 for the red granite. $T_{DM}$ values for the orange granite and nodules range from 2601–2804 Ma, from 2383–2771 Ma for the white leucogranite and from 2433–3079 Ma for the red granites (Table 3).

**Table 3. Sm–Nd isotopic data for selected samples from Point Riley, Black rock and Wallaroo North Beach. Sample location shown in Figures 1c and 2.**

| Sample No. | Granite Phase | Age (Ma) | Sm (ppm) | Nd (ppm) | $^{147}Sm/^{144}Nd$ | $^{143}Nd/^{144}Nd$ | 2se | $\varepsilon_{Nd}(0)$ | $\varepsilon_{Nd}(i)$ | $T_{DM}$(Ma) |
|---|---|---|---|---|---|---|---|---|---|---|
| **2147276** | Orange | 1590 | 3.7 | 16.9 | .1315 | .510239 | 0.000001 | –19.98 | –6.73 | 2804 |
| **2147281** | Orange | 1590 | 0.5 | 2.4 | .1294 | .510315 | 0.000011 | –18.94 | –5.25 | 2641 |
| **2147273** | Nodule | 1590 | 14.3 | 62.1 | .1390 | .510402 | 0.000002 | –15.27 | –3.55 | 2601 |
| **2147272** | White | 1585 | 4.6 | 21.3 | .1296 | .510466 | 0.000001 | –16.04 | –2.42 | 2383 |
| **2147277** | White | 1585 | 1.1 | 4.3 | .1561 | .510090 | 0.000003 | –17.98 | –9.78 | 2771 |
| **2147282** | Red | 1580 | 2.34 | 13.4 | .1098 | .510326 | 0.000002 | –22.85 | –5.29 | 2439 |
| **2149822** | Red (North Beach) | 1580 | 0.8 | 2.9 | .1663 | .509891 | 0.000003 | –19.89 | –13.81 | 3079 |
| **2149823** | Red (Black Rock) | 1580 | 15.5 | 84.7 | .1105 | .510334 | 0.000002 | –22.56 | –5.13 | 2433 |

*$^{147}Sm/^{144}Nd$ CHUR T=0 – 0.1966 (Goldstein et al., 1984)*
*$^{147}Sm/^{144}Nd$ DM T=0 – 0.2145 (Goldstein et al., 1984)*
*$^{143}Nd/^{144}Nd$ CHUR T=0 – 0.512638 (Goldstein et al., 1984)*
*$^{143}Nd/^{144}Nd$ DM T=0 – 0.513150 (Goldstein et al., 1984)*

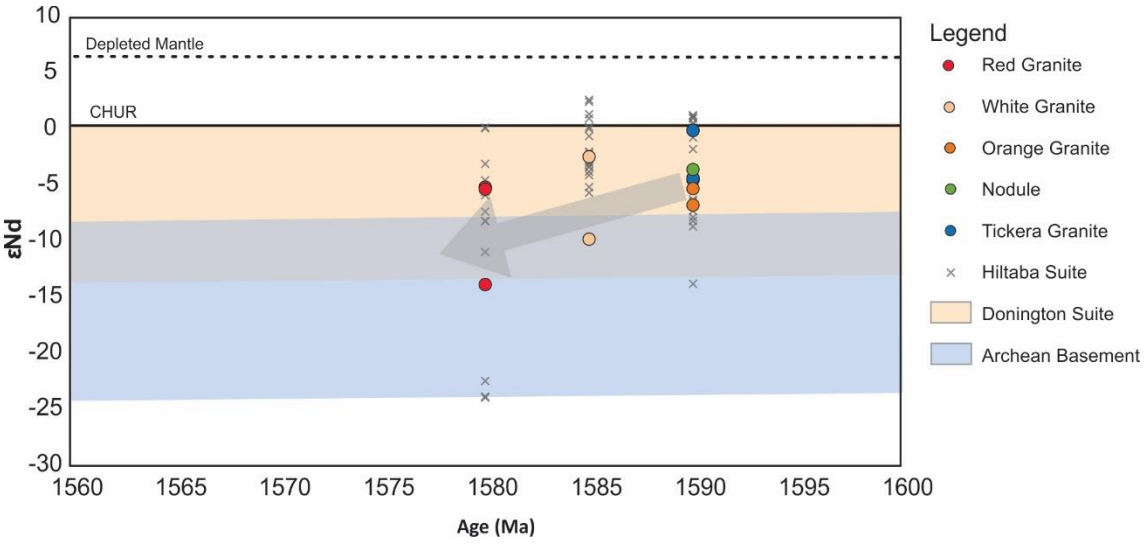


**Figure 11. εNd evolution diagram for granite phases at Point Riley, Black Rock and Wallaroo North Beach. Sample locations are shown in Figures 1c and 2. Data for the surrounding Tickera Granite (Giles 1980; Creaser 1989; Wurst 1994) and for Hiltaba Suite granites from other domains (Creaser 1989; Foden & Stewart 2005; Budd & Skirrow 2007; Skirrow et al., 2007; Rusak 2009) are also shown. Fields for the Donington Suite (Mortimer 1984; Creaser 1989; Turner et al., 1993; Bendall 1994; Schaefer 1998) and Archean Basement (Cooyerdroo Granite and Sleaford Complex; Turner et al., 1993; Swain et al., 2005; Fraser et al., 2010; OZCHEM; SARIG) are also displayed.**

# DISCUSSION

## Relative timing of emplacement of granitic phases

The granitic nodules observed at Point Riley have similar mineralogy and chemistry to the intensely foliated orange granite that hosts them (Figs. 6, 7 and Table 2); however, they differ in degrees of relief due to weathering (Fig 3a). Granitic nodules similar in appearance to those observed at Point Riley have previously been described as granitic 'corestones', which are spherical masses surrounded by weathered rock of the same composition (Twidale & Vidal Romani 2005; Hirata et al., 2016). Corestones form as a result of spheroidal and chemical weathering (hydrolysis) in hard uniform rocks with well–developed joint patterns over an extended period of time (Ollier 1967; Hirata et al., 2016). The similarity of the Point Riley nodules in mineralogy, chemistry, and deformation style to the hosting orange granite, and the morphology of the nodules

suggests that the nodules are corestones, and are therefore the same phase as the orange granite.

Contact relationships are often used to infer relative timing of emplacement of granitic phases. Apophyses have previously been described as contact features between igneous phases, and have been used to demonstrate that the phase containing the apophyses is the relatively younger phase (e.g. De Wet et al., 1989). Apophyses observed at the contact boundary of the white leucogranite and the orange granite (Figs. 2 and 3c) indicate that the orange granite was emplaced before the white leucogranite.

A contact metamorphic boundary preserved in the centre of the study area that shows thermal alteration of the white leucogranite by the red granite (Figs. 2 and 3e), suggesting the red granite is younger than the white leucogranite. However, in the northeast part of the study area, magma mingling between the red and white granite phases is observed (Figs. 2 and 3h). Magma mingling develops when two magmas partially mix and likely takes place both at and en route to the emplacement site (Snyder et al., 1997; Vernon et al., 1998), and has been interpreted to represent coeval magmatism (Medeiros et al., 2001). Evidence of magma mingling between the white leucogranite and red granite in the Point Riley area suggests that these two phases may locally be coeval.

A raft of the white leucogranite is preserved within the red granite dyke (Figs. 2 and 3f). This raft may have formed from melting of the white leucogranite as the red granite intruded, mingling of the two magmas (Vernon et al., 1998), or due to a 3–dimensional feature being exposed on a 2–dimensional rock platform. Evidence of separate and coeval timings of emplacement of the red and white granite phases indicates that the white leucogranite was both locally crystalline and partially molten when the red granite

intruded, suggesting the red granite intruded at the waning stages of white leucogranite magmatism. Overall, the intensely foliated orange granite and nodules are interpreted to be the same phase and are the oldest granites exposed in the Point Riley area. These were intruded by the white leucogranite, and then the youngest phase; the red granite.

## Petrogenesis of Point Riley Granites

Geochemical data can be used to model the source and evolution of magmas (Winter 2010; Hertogen & Mareels, 2016). Granitic phases crystallising from the same magma chamber will cause the residual magma to become progressively more silica–rich through fractional crystallisation, therefore older granite phases will have the lowest $SiO_2$ content (Winter 2010; Hertogen & Mareels, 2016). As plagioclase has a higher melting temperature relative to K–feldspar and quartz, it is also expected that the older granite phases will have higher Ca and Na content relative to younger granite phases. At Point Riley, the orange and white granites show an increasing trend in $SiO_2$ where the white leucogranite is more $SiO_2$ rich, suggesting it represents the younger phase if both phases were from derived the same evolving source. Conversely, the red granite has the broadest $SiO_2$ content, which overlaps with the $SiO_2$ range of the orange and white granites (Figs. 6 and 7), suggesting the red granite could be from another source. However, no other geochemical data supports this notion. The orange to red granite phases show a decrease in Ca and Na content with decreasing $SiO_2$, however the white leucogranite shows the opposite trend (Fig. 6f, g), which is likely due to the high modal proportion of plagioclase in this phase. Additionally, the orange and red granites have higher $K_2O$ content as they are predominantly K–feldspar rich. Additionally, the white leucogranite preserves relatively low $Fe_2O_3$ content and is a slight outlier in $Al_2O_3$

content (Fig. 6a, e). These geochemical variances are likely a result of distinctive differences in mineralogy and alteration as the white leucogranite contains negligible amounts of K–feldspar or hematite alteration, unlike the other granite phases. Based on these differences in mineralogy and geochemistry, it is inferred that the white leucogranite is from a different source region to the orange and red granite phases. Enriched light rare earth element (LREE) content in granites is considered indicative of higher degrees of crustal contamination as LREEs are more abundant in the crust while heavy rare earth elements (HREE) are more abundant in the mantle (Walters et al., 2013). Overall, the nodules, orange and red granite phases exhibit similar REE patterns showing enriched LREE contents and high LREE/HREE ratios (Table 2; Fig. 10). This supports the conclusion that these phases are from a similar crustal source region, although indication of locally variable sources are evident from the comparatively different REE patterns within the granite phases (Fig. 10). The white leucogranite preserves a significantly different REE pattern showing relatively lower LREE/HREE ratios compared to the other granite phases, suggesting a more mafic source. Positive Eu anomalies infer less fractionation of plagioclase and may have been inherited from a source that was characterised by positive Eu anomalies, while negative Eu anomalies suggests fractionation of plagioclase during formation (Winter 2010). One white and one orange granite sample (samples 2147277 and 2147281 respectively) display relatively flat to positive Eu anomalies and relatively low LREE/HREE ratios (Fig. 10), suggesting the incorporation of a more mafic material. Alternatively, the remainder of the samples are characterised by negative Eu anomalies, suggesting a crustal source. Two red granites and one nodule display high degrees of plagioclase fractionation but relatively low LREE/HREE ratios (Fig. 10), which also infers

incorporation of more mafic or lower crustal material into these phases. These interpretations suggest the granite phases do not solely have an evolved crustal source, rather a more variable source including amalgamation of a lower crustal and/or mafic material.

Sm–Nd isotopes can be used to determine the source region of magmas and the relative contribution of crustal versus mantle material (e.g. DePaolo et al., 1992). The εNd values for the samples analysed in this study cover a broad range from –2.44 to –13.81 (Fig. 11). Previously published εNd values for samples of the Tickera Granite which were taken from the sample pluton in the Moonta region (Giles 1980; Creaser 1989; Wurst 1994), show similar values despite having an older model age (Fig. 11). Overall, the phases of Tickera Granite in the Moonta region show increasingly negative εNd(i) values over time, which is indicative of progressive input of crustal material throughout magma evolution. This is likely due to the assimilation and fractional crystallisation of the surrounding wall rock as the magma ascends and evolves. One sample of the white leucogranite has a more juvenile εNd value (–2.42: 2147272) than the other granite phases, indicating some input from a more mafic source.

Overall, the mineralogy, geochemical and isotopic data for the Tickera Granite suggests that the nodules, orange and red granite phases are from a similar source, and the white leucogranite is from a slightly different, more mafic source region. Possible sources for the Tickera Granite in the Moonta Domain includes the underlying Wallaroo Group and Donington Suite. The εNd values for the Donington Suite partially overlap with the Point Riley samples (Fig. 11), and are general relatively juvenile, therefore is unlikely to be the sole source of the Tickera Granite. The Archean basement underlying the Wallaroo Group and Donington Suite is also considered as potential source region. The

εNd values of Archean basement (the Mesoarchean Cooyerdoo Granite and Neoarchean Sleaford Complex) ranges from approximately –8 to –24 (Turner et al., 1993; Swain et al., 2005; Fraser et al., 2010; Fig. 10), and are significantly more evolved than the majority of the samples analysed in this study (Fig. 11).

εNd data indicates that the Donington Suite is a likely source for the Tickera Granite. However, it is difficult to assess the potential input from the Wallaroo Group as there is currently no εNd data available. Variable REE content of the granite phases suggests input from a crustal source of variable nature. The Wallaroo Group which includes psammites, siltstones, calcsilicates, albitites, quartzites, iron rich sediments and volcanics (e.g Cowley et al., 2003) has the potential to produce melt with variable REE content (and therefore εNd values), and cannot be discounted as a potential source region. Similarly, the Donington Suite comprises igneous rocks of mafic to felsic composition, which also has the potential to produce variable REE content and εNd values. Based on the εNd and REE data, it is suggested that the Tickera Granite may be derived from the Donington Suite and/or Wallaroo Group with some input from a more mafic or lower crustal source, which could potentially be the underlying Archean basement.

## Comparison with the broader Hiltaba Suite

The Tickera Granite is generally inferred to be part of the Hiltaba Suite granites (e.g. Conor 1995; Conor et al., 2010). Comparison of whole rock geochemical data for samples of the Tickera Granite collected in this study with published data from Hiltaba–aged (ca. 1595–1575 Ma) granites of the Moonta Domain (Fig. 1b) shows similar trends. Major and trace element data generally overlaps, with the exception of a cluster

of samples for the Moonta Domain that are elevated in $P_2O_5$, MgO and $TiO_2$ (Fig. 6b–d), and Sc, Th, Ce and La (Fig. 7b, c, e, f). These differences are likely due to samples being taken from the Arthurton Granite and slight differences between plutons in the Moonta region, but can generally be inferred to be of similar composition.

Comparison of the Tickera Granite samples from this study with the broader Hiltaba Suite granites from the Olympic, Wilgena and Nuyts Domains (Fig. 1b) shows that the data defines similar linear trends for most major and trace elements. Differences in chemistry of Hiltaba Suite granites between domains has previously been studied by Stewart & Foden (2003). The Moonta Domains considered to preserve elevated Th concentrations, and depleted CaO, Sr and MnO concentrations compared to the rest of the suite (Stewart and Foden 2005). The samples used in this study generally support this interpretation however, few of the samples show relatively high Sr values compared to the Moonta Domain and the rest of the Hiltaba Suite. However, the white leucogranite mapped at Point Riley has elevated $Na_2O$ and depleted $K_2O$ concentrations compared to other data from the Tickera Granite and broader Hiltaba Suite, with the exception of 3–4 data points from the Moonta Domain and three samples from the Wilgena Domain (Fig. 6k), which is attributed to this phase being plagioclase rich. Similarly, the high Ca/low K concentrations for samples of the white leucogranite at Point Riley is attributed to this phase being plagioclase rich and K-feldspar-poor (Fig. 6j). In general, the plagioclase-rich nature of the white leucogranite contrasts with the typically K-feldspar-rich nature of the Hiltaba Suite granites (e.g. Daly et al., 1993; Stewart & Foden 2003). Data in this study has also shown that the white leucogranite is from a different source to the other phases observed at Point Riley. Comparison of εNd

signatures of the Tickera Granite samples of this study with the broader Hiltaba Suite granites shows that the data are broadly comparable, (Fig. 11).

Similar major, trace element and isotopic data between the Tickera Granite and the majority of the Hiltaba Suite supports the notion that the Tickera Granite is part of the broader Hiltaba Suite. However, it is noted that there are localised phases within the Moonta Domain (including the Tickera Granite) and Wilgena Domain that suggests they were derived from a slightly different source region compared to the broader Hiltaba Suite. This is supported by Stewart and Foden (2005) who suggests that the Hiltaba Suite is a combination of mantle and crustal material, with the crustal component being less than 30%, and variations related to different amounts of compositions of mantle and crustal endmembers.

## Structural fabrics and deformation style within Yorke Peninsula

The mechanisms by which deformation is accommodated in granites depends on a number of variables including crustal level of emplacement, granite rheology and morphology (e.g. Evans 1988; Tobisch & Paterson 1998). At higher metamorphic grades foliations develop, while at lower grades cleavages develop (Winter 2010). Structures can also manifest differently as a result of a composite of structures from progressive deformation events (Tobisch & Paterson 1998). A well–developed northeast–trending foliation is preserved in the orange granite and locally in the red granite (Figs. 3a, b and 4a, c). Conversely, the white leucogranite preserves a well–developed cleavage in the same northeast–trending orientation (Figs. 3d and Fig. 4b). The pervasive northeast-trending fabrics observed may have developed in the same deformation event, however, have manifested differently in the granite phases due to

differences in rheology, emplacement depths and/or due to a combination of structures from multiple deformation events.

Evidence of emplacement of the red granite at shallow crustal levels is demonstrated by the local preservation of cavities within this granite phase (Fig. 2, 3g). These cavities have been suggested to be miarolitic cavities (Conor et al., 2010), which develop during uplift as pockets of gas expand within a magma, and are therefore indicative of emplacement at shallow crustal levels (Petford 2003). The presence of these cavities in the red granite suggests this phase was emplaced at shallow crustal levels, supporting the suggestion that the degree of preservation of the dominant northeast–trending fabric in the Point Riley area is variable due to the variation of crustal levels where the granites were emplaced. However, it is noted that these features have not indisputably been demonstrated to be miarolitic cavities, but may have resulted from other processes such as weathering and the removal of K–feldspar phenocrysts. Similar cavities have been reported in the Arthurton Granite, and are interpreted to have resulted from exsolution of magmatic volatile phases (Zang et al. 2007).

The preservation of the northeast–trending foliation along the margins of the red granite, combined with the knowledge that magmas crystallise from the outer edges inwards (Winter 2010), suggests that the initial stages of emplacement of the red granite may have occurred during the waning stages of this deformation event. These northeast–trending structures are also subparallel to the orientation of the shoreline at Point Riley, and have been correlated with a major northeasterly trending structure just off–shore (Conor et al., 2010).

The northeast–trending fabric has also been observed in the Wallaroo Group metasediments in the Point Riley area (Wurst 1994; Arcaro 2000; Zang et al., 2006;

Conor et al. 2010), and is also seen as a strongly developed northeast–trending structural grain across the Yorke Peninsula (e.g. Wurst 1994; Arcaro 2000; Conor 2002; Conor et al. 2010; Conor 2016). This fabric may be associated with the later deformation event described by Conor et al., (2010) that resulted in development of northeast–trending upright folds. In the Wallaroo North Beach area, exposures of the upright folds are preserved within the Wallaroo Group metasediments, where they are observed to be refolding an earlier generation of isoclinal folds to produce a Type 3 fold interference pattern (See Plate 38 in Conor 2016; Wurst 1994; Arcaro 2000; Conor et al. 2010). Development of Type 3 fold interference patterns implies the axial trace of the earlier fold generation was subparallel to the axial trace of the overprinting fold generation, and that the axial plane of the folds were at a high angle (Ramsay 1962). This implies that the earlier isoclinal fold generation in the Point Riley area had a northeast trending axial trace and a shallowly inclined to recumbent axial plane, and that the northeast–trending fabric may be a composite of the earlier isoclinal folds and the later upright folds. The mechanism for development of recumbent folds with a northeast trending axial trace would likely be northwest–southeast directed shortening.

Long–limbed, upright, tight to isoclinal folds with northeast–trending fold axial planes have been described in the eastern Yorke Peninsula from aeromagnetic imagery (Parker 1993; Wurst 1994; Conor 2002; Conor et al., 2010). The relationship between these isoclinal folds and the northeast–trending upright folds observed in the Wallaroo Group in northwestern Yorke Peninsula is unknown, however the northeast–trending orientation supports the notion that the two fold generations observed in the Yorke Peninsula may have produced a composite northeast–trending fabric that is seen throughout the region.

A second, poorly– to moderately–developed, northwest–trending cleavage is preserved within all granite phases at Point Riley at different degrees, and overprints the dominant foliation seen in the orange and red granites (Fig. 2, 3c, d, f). This cleavage is interpreted to have developed during a later deformation event, possibly when the granites in the Point Riley area were at shallower crustal levels where deformation is accommodated via cleavage rather than foliation development. Northwest–trending structures including conjugate faults, fractures and shear zones have been recognised in the western Yorke Peninsula (e.g. Arcaro 2000; Zang et al., 2006; Conor et al. 2010) and in aeromagnetic magnetic imagery (Conor 2002; Conor 2016). Formation of these structures are suggested to be a product of emplacement of the Tickera Granite, resulting in mineralisation in the region (e.g. Dickinson 1953; Wurst 1994; Zang et al., 2006; Conor et al., 2010). The similar orientation of cleavages at Point Riley and regional structures in the northwestern Yorke Peninsula suggests that later deformation may have been localised, and occurred subsequently after granite emplacement. .

Few studies have been done to compare structural fabrics preserved within the Tickera Granite to the surrounding Wallaroo Group (e.g. Wurst 1994, Arcaro 2000), and to relate the timing of deformation within the granites and the hosting metasediments (Wurst 1994; Arcaro 2000; Conor et al. 2010). The timing of deformation events that effected the Tickera Granite has generally been constrained to be synchronous with the timing of intrusion of the Point Riley granite phases at ca. 1597–1577 Ma (Conor 1995). This implies that the later northeast–trending upright folds developed at this time. This correlation and interpreted timing of deformation is supported by Conor et al. (2010), who suggest that the later upright folds are attributed to deformation associated with intrusion of the Hiltaba Suite granites.

The timing of the earlier isoclinal fold event is equivocal, and has been inferred to be related to the ca. 1730–1690 Ma Kimban Orogeny (Conor et al. 2010). This conclusion is based on the absence of amphibolite–rich calc–silicate alteration in the isoclinal folds, which is observed within the upright fold generation and is interpreted to be associated with the Hiltaba Suite event (Conor et al., 2010). This suggests deformation of the two fold generations may have occurred during the Kimban Orogeny, but does not exclude the possibility that the isoclinal folds developed just prior to initial stages of granite intrusion at ca. 1595 Ma and generation of the upright folds. The latter may overlap with the timing of intense deformation and metamorphism across eastern Proterozoic Australia, including the Gawler Craton and Curnamona Province at ca. 1600–1580 Ma (e.g. Page et al. 2005; Hand et al., 2007; Forbes et al., 2008, 2012; Fig. 12).

## Relationships with the northern Gawler Craton and Curnamona Province

The late Palaeo to early Mesoproterozoic marked a significant period of metamorphism, deformation, magmatism and mineralisation within eastern Proterozoic Australia (e.g. Collins & Shaw 1995; Betts et al., 2002; Giles & Nutman 2002; Hand et al. 2007; Forbes et al., 2008; Stewart & Betts 2010; Forbes et al., 2012). Within southern Proterozoic Australia, this event is unnamed, but is recognised within the Gawler Craton (e.g. Hand et al. 2007; Szpunar et al. 2007; Cutts et al. 2011; Forbes et al. 2011, 2012; Morrissey et al. 2014), and is identified as the ca. 1600–1585 Ma Olarian Orogeny within the Curnamona Province (e.g. Page et al. 2005; Forbes et al. 2008; Fig. 12.

Within the northern Gawler Craton, the metamorphic regime at ca. 1600–1580 Ma is well defined (e.g. Szpunar et al. 2007; Cutts et al. 2011; Forbes et al. 2011, 2012;

Morrissey et al. 2014), however the deformational regime at this time is not. Deformation within the Mount Woods Inlier in the northeastern Gawler Craton (Fig. 1b) may have resulted in development of isoclinal folds during the Kimban Orogeny (Betts et al. 2003), or leading up to/synchronous with emplacement of the ca. 1584 Ma Balta Granite Suite (O'Sullivan 2010). Subsequent deformation involved the uplift and exhumation of the Mount Woods Inlier along the Southern Overthrust, which was initiated at ca. 1592–1582 Ma (Forbes et al., 2012).

Although the timing of the early isoclinal folding event in the Mount Woods Inlier is conjectural, it shares similarities to the early deformation history observed in the Yorke Peninsula. However, later generation of open upright folds similar to that observed in the Yorke Peninsula, has not been recognised in the Mount Woods Inlier. Overall, the lack of constraint on the Proterozoic deformational regime of the Gawler Craton, makes correlation with the deformation history of the Yorke Peninsula difficult.

The geological history of the Curnamona Province (Fig, 1b) at 1600–1580 Ma is better constrained, and shows a similar history to the Yorke Peninsula. Early isoclinal, recumbent (nappe) folds are interpreted to have developed during northwest–directed thrusting. The early folds were overprinted by northeast trending, open, upright folds during upper amphibolite to granulite–facies metamorphism as a result of northwest–southeast directed shortening (Marjoribanks et al., 1980; Hobbs et al., 1984; Forbes et al., 2004, 2005, 2007; Page et al., 2005). In the northern Broken Hill Inlier, overprinting of the fold generations lead to the development of Type 2 and Type 3 fold interference patterns (Forbes & Betts 2004; Forbes et al., 2004). The generation of open upright folds is also responsible for the dominant north–south structural grain throughout the Broken Hill Block (Forbes et al., 2004). Granites intruded the Curnamona Province

synchronously with and immediately following the deformation events, and include the ca. 1600–1570 Ma Ninnerie Supersuite (Page et al. 2005; Wade 2011), which was emplaced during the generation of the later upright folds (Gibson et al., 2004; Page et al. 2005). Granites of the Ninnerie Supersuite is interpreted to be equivalents of the 1595–1575 Ma Hiltaba Suite (Hand et al., 2008; Conor et al., 2010; Conor 2016).

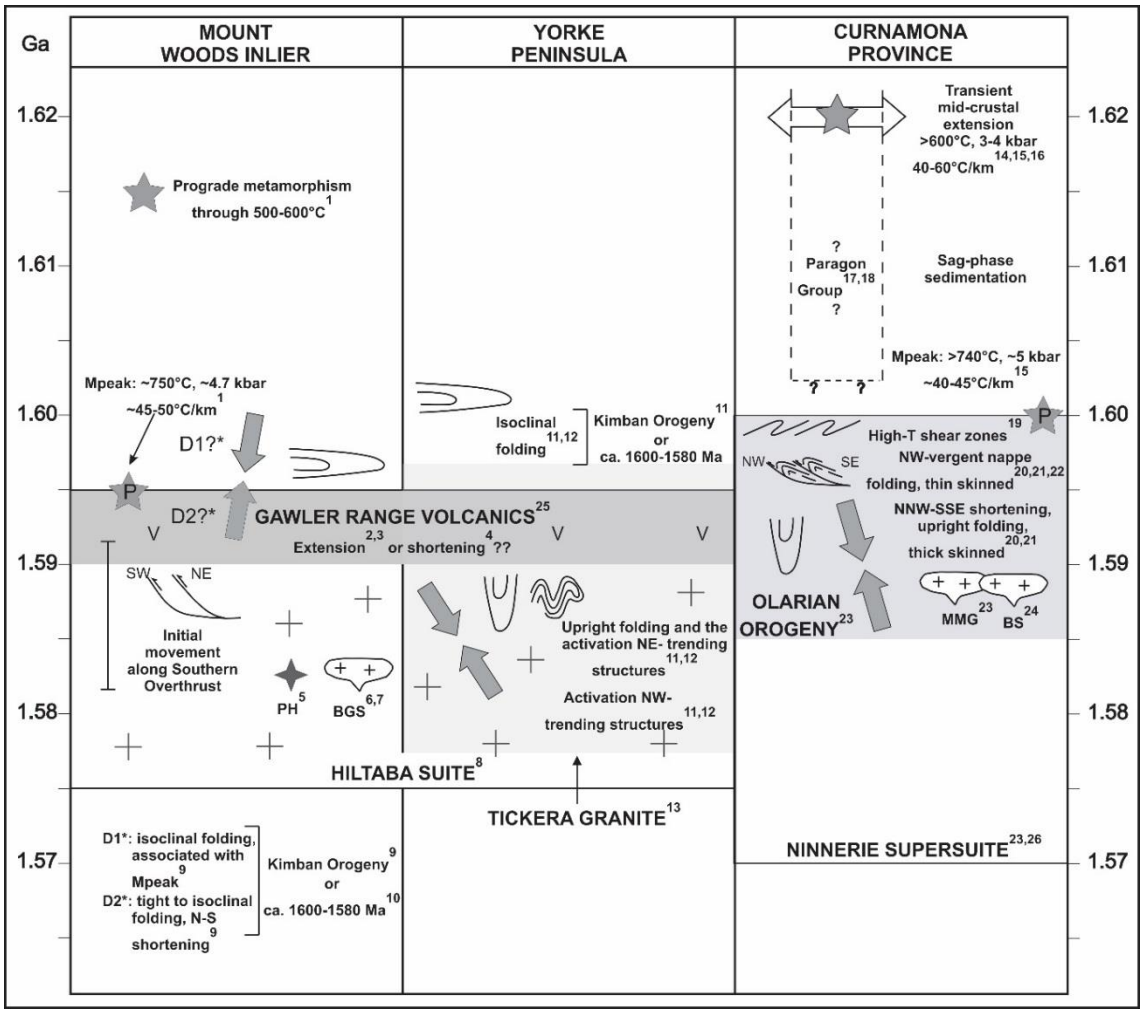


**Figure 12. 1620–1570 Ma cladogram of selected Proterozoic terranes in South Australia, modified from Forbes et al. (2012). This includes the Mount Woods Inlier in the northern Gawler Craton, Yorke Peninsula in the southeastern Gawler Craton, and the Curnamona Province. Mineralisation: PH: Prominent Hill. Intrusives: BGS: Balta Granite Suite; MMG: Mundi Mundi Granites; BS: Bimbowrie Suite. References: Forbes et al. (2011); 2. Hitzman et al. (1992); 3. Betts et al. (2009); 4. Direen and Lyons (2007); 5. Belperio et al. (2007); 6. Fanning (1993); 7. Finlay (1993); 8. Creaser and Cooper (1993); 9. Betts et al. (2003); 10. O'Sullivan (2010); 11. Conor et al. (2010); 12. Hand et al. (2007); 13. Conor (1995); 14. Forbes et al. (2008); 15. Forbes et al. (2005); 16. Forbes et al. (2007); 17. Raetz et al. (2002); 18. Page et al. (2000); 19. Forbes et al. (2012); 20. Forbes et al. (2004); 21. Forbes and Betts (2004); 22. Gibson et al. (2004); 23. Page et al. (2005); 24. Ludwig and Cooper (1984); 25. Fanning et al. (1998); 26. Wade (2011).**

Overall, the timing of at least one deformation event, the general orientation of structures and the timing of magmatism in the Yorke Peninsula and the Curnamona Province are similar. Both regions preserve evidence of two deformation events which have generally been constrained to similar times, and resulted in the development of a north–northeast trending structural grain within each region. In addition, if the generation of early isoclinal folds in the Yorke Peninsula occurred just prior to granite intrusion, these regions would share an even closer deformation history. Constraint on the timing of the earlier isoclinal folding in the Yorke Peninsula is needed to unequivocally determine the extent in similarity between the two regions.

## CONCLUSIONS

The Tickera Granite is part of the broader Hiltaba Suite and comprises three phases; an early intensely foliated orange granite that was intruded by a white leucogranite and a later red granite. These localised phases differ compositionally, geochemically and isotopically, suggesting a heterogeneous source region. The white leucogranite originated from a similar but slightly more mafic source. Derivation of the Tickera Granite is likely from the Donington Suite and/or Wallaroo Group, with slight contamination from the underlying Archean basement.

The northeast–trending structures preserved at Point Riley are interpreted to be a composite fabric as a result of early isoclinal folds that were overprinted by open, upright folds. Early isoclinal folding is suggested to have occurred during the Kimban Orogeny or leading up to emplacement of the Tickera Granite at ca. 1597–1577 Ma. These northeast–trending structures are correlated with a regional northeast–trending fabric that defines the dominant structural grain across the Yorke Peninsula.

The Yorke Peninsula shares a similar deformational and magmatic history to the ca. 1600–1585 Ma Olarian Orogeny in the Curnamona Province, whereby each region preserves evidence of two deformation events, a dominant northeast trending structural grain and spatially and temporally related granite intrusions. Further constraint on the timing of early isoclinal folding in the Yorke Peninsula is required to determine the extent of similarities between the regions geological histories.

## ACKNOWLEDGMENTS

Foremost I would like to thank Dr Caroline Forbes for her unwavering support, knowledge and supervision throughout the year. You're a true legend! Secondly I would like to thank my co-supervisor Dr Anthony Reid for his advice and guidance, Claire Wade for her knowledge and constant support, and Colin Conor for his valuable insights throughout the year. Many thanks to the Geological Survey of South Australia for this project opportunity and support. To David Bruce for your guidance and patience when everything that could go wrong, did. Katie Howard, for her optimism as the Honours Support Officer. To Alan Collins and John Foden for organising this year's trip to New Zealand. Shauna and Maria for the company on my field trips and the many late nights in the office. To my Honours cohort, thanks for making this year worth it! And lastly, to Juraj Farkas and the geology faculty staff who always made spare time and provided support when needed.

## REFERENCES

ARCARO, H. D. (2000). Structure of the Proterozoic Assemblages of Point Riley and North Beach: Tectonic Environment of Formation. (Bachelor of Science), Monash University, Unpublished.

BETTS, P. G., GILES, D., LISTER, G. S., FRICK, L. R. (2002). Evolution of the Australian lithosphere. *Australian Journal of Earth Sciences, 49*(4), 661-695

BETTS, P.G., VALENTA, R.K., & FINLAY, J., (2003). Evolution of the Mount Woods Inlier, northern Gawler Craton, Southern Australia: an integrated structural and aeromagnetic analysis. *Tectonophysics*, 366, 83–111.

BETTS, P.G., GILES, D., FODEN, J., SCHAEFER, B.F., MARK, G., PANKHURST, M.J., FORBES, C.J., WILLIAMS, H.A., CHALMERS, N.C., HILLS, Q.G., (2009). Mesoproterozoic plumemodified orogenesis in eastern Precambrian Australia. Tectonics 28, TC3006, doi:10.1029/2008TC002325.

BELPERIO, A., FLINT, R., FREEMAN, H., (2007). Prominent Hill: a hematite-dominated, iron oxide copper–gold system. *Economic Geology* 102, 1499–1510.

BUDD, A. (2006). A- and I-type subdivision of the Gawler Ranges-Hiltaba Volcano-Plutonic Association. *Geochimica Et Cosmochimica Acta*, *70*(18), A72.

BUDD, A. & SKIRROW, R. (2007). The Nature and Origin of Gold Deposits of the Tarcoola Goldfield and Implications for the Central Gawler Gold Province, South Australia. *Economic Geology, 102*(8), 1541-1563.

COLLINS, W. J., & SHAW, R. D. (1995). Geochronological constraints on orogenic events in the Arunta Inlier: a review. *Precambrian Research, 71*(1–4), 315-346.

CONOR, C.H.H., (1995). Moonta-Wallaroo Region - An interpretation of the geology of the Maitland and Wallaroo 1:100 000 sheet areas. *In M. a. E. S. Australia* (Ed.), (pp. 1-100).

CONOR, C.H.H., (2002). The Palaeo-Mesoproterozoic geology of northern Yorke Peninsula, South Australia: Hiltaba Suite-related alteration and mineralisation of the Moonta-Wallaroo Cu-Au District. *Geological Field Guidebook, Geological Survey of South Australia,* Report Book 2002/007

CONOR, C.H.H., (2003). An early Mesoproterozoic FeO-Cu-Au province – hints of its global extent. *MESA Journal*, v. 29, pp 42-45

CONOR, C. H. H., & PREISS, W. V. (2008). Understanding the 1720–1640 Ma Palaeoproterozoic Willyama Supergroup, Curnamona Province, Southeastern Australia: Implications for tectonics, basin evolution and ore genesis. *Precambrian Research, 166*(1), 297-317.

CONOR, C., RAYMOND, A. L., BAKER, T., TEALE, G., SAY, P., LOWE, G. (2010). Alteration and Mineralisation in the Moonta-Wallaroo Copper-Gold Mining Field Region, Olympic Domain, South Australia. *Hydrothermal Iron Oxide Copper-Gold and Related Deposits, 3*, 147-170.

CONOR, C.H.H., (2016). Geological Field Excursion Guide — IOCGs – Where it all began: The Moonta-Wallaroo region of the eastern Gawler Craton, Report Book 2016/00009. Department of State Development, South Australia; and Geological Society of Australia, South Australian Division.

COWLEY, W.M., & FANNING, C.M., (1991). Low-grade Archaean metavolcanics in the northern Gawler craton: *Geological Survey of South Australia, Quarterly Geological Notes*, v. 119, p. 2–17.

COWLEY, W. M., CONOR, C., & ZANG, W. L. (2003). New and revised Proterozoic stratigraphic units on northern Yorke Peninsula. *MESA Journal, 29*, 46-58

CREASER, R. A., & COOPER, J. A. (1993). U-Pb Geochronology of Middle Proterozoic Felsic Magmatism Surround the Olympic Dam Cu-U-Au-Ag and Moonta Cu-Au-Ag deposits, South Australia. *Economic Geology, 88*, 186-197

CUTTS, K.A., HAND, M., & KELSEY, D.E., (2011). Evidence for early Mesoproterozoic (ca. 1590 Ma) ultrahigh-temperature metamorphism in southern Australia. *Lithos* 124, 1–16.

DALY, S.J., AND FANNING, C.M., (1993), Archaean, *in* Drexel, J.F., Preiss, W.V., and Parker, A.J., eds., *The Geology of South Australia; Volume 1, The Precambrian: South Australia Geological Survey, Bulletin* 54, p. 32–49.

DALY, S.J., FANNING, C.M., & FAIRCLOUGH, M.C., (1998). Tectonic evolution and exploration potential of the Gawler craton, South Australia. *AGSO Journal of Australian Geology and Geophysics*, v. 17, p. 145–168.

DE WET, A., MILLER, J., BICKLE, M., CHAPMAN, H. (1989). Geology and geochronology of the Arnea, Sithonia and Ouranopolis intrusions, Chalkidiki peninsula, northern Greece. *Tectonophysics*, 161(1-2), 65-79.

DEPAOLO, D., PERRY, F., & BALDRIDGE, W. (1992). Crustal versus mantle sources of granitic magmas: a two-parameter model based on Nd isotopic studies. *Earth And Environmental Science Transactions Of The Royal Society Of Edinburgh*, *83*(1-2), 439-446.

DICKINSON, S.B., (1953). The Moonta and Wallaroo copper mines; in *Geology of Australia Ore Deposits: 5th Empire Mining and Metallurgical Congress, Australia and New Zealand, Publications*, v. 1, pp. 487-504

DIREEN, N.G., & LYONS, P., (2007). Regional crustal setting of iron oxide Cu–Au mineral systems of the Olympic Dam region, South Australia: insights from potentialfield modelling. Economic Geology 102, 1397–1414.

DUTCH, R., HAND, M. & KINNY, P. D., (2008). High-grade Paleoproterozoic reworking in the southeastern Gawler Craton, South Australia. *Australian Journal of Earth Sciences*, 55: 1063-1081.

EVANS, J. (1988). Deformation mechanisms in granitic rocks at shallow crustal levels. *Journal Of Structural Geology*, *10*(5), 437-443.

FANNING, C. M., FLINT, R. B., PARKER, A. J., LUDWIG, K. R., & BLISSETT, A. H. (1988). Refined Proterozoic evolution of the Gawler Craton, South Australia, through U-Pb zircon geochronology. *Precambrian Research, 40*(41), 363-386

FANNING, C.M., (1993). Ion-microprobe U–Pb zircon dating of the Mount Woods Inlier, Preliminary Results (Unpublished). Research School of Earth Sciences, Australian National University, 8 pp

FANNING, C. M., (1997). Geochronological synthesis of southern Australia: Part II, The Gawler Craton. *Department of Primary Industries and Resources South Australia*, ENV 08918 (unpublished): 24–76.

FANNING, C. M., REID, A., & TEALE, G. (2007). A geochronological framework for the Gawler Craton, South Australia. *Geological Survey, Bulletin 55*.

FERRIS, G.M., SCHWARZ, M.P., & HEITHERSAY, P., (2002). The geological framework, distribution and controls of Fe-oxide and related alteration, and Cu-Au mineralisation in the Gawler craton, South Australia. Part I: geological and tectonic framework, *in* Porter, T.M., ed., Hydrothermal iron oxide copper- gold and related deposits: A global perspective, 2: Adelaide, *Porter GeoConsultancy Publishing*, p. 9–31.

FINLAY, J., (1993). Structural interpretation of the Mount Woods Inlier. Honours Thesis (unpub.), Monash University, Australia

FLINT, R.B., BLISSETT, A.H., CONOR, C.H.H., COWLEY, W.M., CROSS, K.C., CREASER, R.A., DALY, S.J., KRIEG, G.W., MAJOR, R B., TEALE, G.S., AND PARKER, A.J., (1993). Mesoproterozoic, *in* Drexel, J.F., Preiss, W. V., and Parker, A. J., eds., *The Geology of South Australia; Volume 1, The Precambrian: South Australia Geological Survey, Bulletin* 54, p. 106–169.

FLINT, R. B. (2002). Structural evolution of the Outalpa Inliers, Olary Domain, Curnamona Province. *MESA Journal, 26*, 34-41

FORBES, C.J., & BETTS, P.G., (2004). Development of Type 2 fold interference patterns in the Broken Hill Block: implications for strain partitioning across a detachment during the Olarian Orogeny. *Australian Journal of Earth Sciences* 51, 173–188.

FORBES, C.J., BETTS, P.G., & LISTER, G.S., (2004). Synchronous development of Type 2 and Type 3 fold interference patterns: evidence for recumbent sheath folds in the Allendale Area, Broken Hill, NSW, *Australia. Journal of Structural Geology*, 26, 113–126

FORBES, C.J., BETTS, P.G., WEINBERG, R., BUICK, I.S., (2005). Metamorphism and high temperature shear zones in the Broken Hill Block, NSW, *Australian Journal of Metamorphic Geol*ogy, 23, 745–770.

FORBES, C.J., GILES, D., BETTS, P.G.,WEINBERG, R., KINNY, P., (2007). Dating prograde amphibolite and granulite facies metamorphism in the Broken Hill Block, NSW, using in situ monazite U-Pb SHRIMP analysis. *J. Geol*. 115, 691–705.

FORBES, C. J., BETTS, P. G., GILES, D., & WEINBERG, R., (2008). Reinterpretation of the tectonic context of high-temperature metamorphism in the Broken Hill Block, NSW, and implications on the Palaeo- to Meso-Proterozoic evolution. *Precambrian Research*, 338-349.

FORBES, C.J., GILES, D., HAND, M., BETTS, P.G., SUZUKI, K., CHALMERS, N., DUTCH, R., (2011). Using P–T paths to interpret the tectonothermal setting of prograde metamorphism: an example from the northeastern Gawler Craton, South Australia. *Precambrian Research*, 185, 65–85.

FORBES, C. J., GILES, D., JOURDAN, F., SATO, K., OMORI, S., & BUNCH, M. (2012). Cooling and exhumation history of the northeastern Gawler Craton, South Australia. *Precambrian Research, 200-203*, 209-238.

FOSSEN, H. (2010). Structural geology. *Cambridge: Cambridge University Press*, page 296.

FRASER, G., SKIRROW, R.G., & HOLM, O., (2007). Mesoproterozoic gold prospects in the central Gawler Craton, South Australia: geology, alteration, fluids and timing. *Economic Geology*, 1511-1539.

FRASER, G.L., & NEUMANN, N., (2010). New SHRIMP U-Pb zircon ages from the Gawler Craton and Curnamona Province, South Australia, 2008–2010: *Geoscience Australia*, Record 2010/16.

FRASER, G., MCAVANEY, S., NEUMANN, N., SZPUNAR, M. AND REID, A., (2010a). Discovery of early Mesoarchean crust in the eastern Gawler Craton, South Australia: *Precambrian Research*, v. 179, pp. 1–21.

GIBSON, G.M., PELJO, M., & CHAMBERLAIN, T., (2004). Evidence and timing of crustal extension versus shortening in the early tectonothermal evolution of a Proterozoic continental rift sequence at Broken Hill, Australia. *Tectonics 23*, TC5012.

GILES, C.W., (1980). A comparative study of Archaean and Proterozoic felsic volcanic associations in southern Australia. PhD thesis, University of Adelaide.

GILES, D., & NUTMAN, A.P., (2002). SHRIMP U–Pb monazite dating of 1600–1580 Ma amphibolite facies metamorphism in the southeastern Mt Isa Block, Australia. *Australian Journal of Earth Sciences 49*, 455–465.

GOLDSTEIN, S.L., ONIONS, R.K. & HAMILTON, P.J. (1984). A Sm-Nd Isotopic Study of Atmospheric Dusts and Particulates from Major River Systems. *Earth and Planetary Science Letters 70(2): 221-236.*

HITZMAN, M.W., ORESKES, N., & EINAUDI, M.T., (1992). Geological characteristics and tectonic setting of Proterozoic iron oxide (Cu–U–Au–REE) deposits. *Precambrian Research* 58, 241–287.

JAGODZINSKI, E.A., (2005). Compilation of SHRIMP U-Pb geochronological data, Olympic Domain, Gawler craton, South Australia, 2001-2003: *Geoscience Australia*, Record 2005/20, p. 211.

JAGODZINSKI, E. A., FREW, R. A., FOUDOULIS, C., BLACK, L., REID, A., ZANG. W., PAYNE, J., SCHWARZ, M. P., (2006). Compilation of SHRIMP U-Pb geochronological data for the Gawler Craton, South Australia 2006. *Primary Industries and Resources South Australia*, Report Book 2006/20: pp. 125

JAGODZINSKI, E. A., REID, A. J., CHALMERS, N. C., SWAIN, S., FREW, R. A., FOUDOULIS, C., (2007). Compilation of SHRIMP U-Pb geochronological data for the Gawler Craton, South Australia, 2007. *South Australia. Department of Primary Industries and Resources*, Report Book, 2007/21: pp. 93.

JAGODZINSKI, E., REID, A.J. & FARRELL, F., (2011a). Project PGC01-05: Geochronology of gneissic, granitic and gabbroic rocks from west of the Middleback Range *in* Reid, A.J. and Jagodzinski, E.A. (eds), PACE Geochronology: Results of collaborative geochronology projects 2009–10: *South Australian Department of Primary Industries and Resources, Report Book* 2011/03, pp. 63–94.

JAGODZINSKI, E. J., REID, A. & FARRELL, F., (2011b). Project PGC01-04: Geochronology of the Bungalow Prospect. *Geological Survey of South Australia*, Report book 2011/003:

JAGODZINSKI, E. & MCAVANEY, S., (2016). SHRIMP U-Pb geochronology data for northern Eyre Peninsula, 2013-2014. *Geological Survey of South Australia*, RB2016/xxx:

HAND, M., REID, A., & JAGODZINSKI, E. (2007). Tectonic Framework and Evolution of the Gawler Craton, Southern Australia. *Economic Geology, 102*, 1377-1395

HAND, M., REID, A., JAGODZINSKI, E., KELSEY, D., PEARSON, N. (2008). Paleoproterozoic orogenesis in the southeastern Gawler Craton, South Australia. *An International Geoscience Journal of the Geological Society of Australia*, *55*(4), 449-471. doi: 10.1080/08120090801888594

HERTOGEN, J. & MAREELS, J. (2016). SilMush: A procedure for modeling of the geochemical evolution of silicic magmas and granitic rocks. *Geochimica Et Cosmochimica Acta*, *185*, 498-527. http://dx.doi.org/10.1016/j.gca.2016.04.044

HIRATA, Y., CHEN, Y., & CHIGIRA, M. (2016). Spheroidal weathering of granite porphyry with welldeveloped columnar joints by oxidation, iron precipitation, and rindlet exfoliation. *Earth Surf. Process. Landforms*.

HOBBS, B.E., ARCHIBALD, N.J., ETHERIDGE, M.A., WALL, V.J., (1984). Tectonic history of the Broken Hill Block, Australia. In: Kröner, A., Greiling, R. (Eds.), Precambrian Tectonics Illustrated. Schweizerbart'sche Verlagsbuchhandlung, Stuttgart, pp. 353–368.

HOEK, J.D., & SCHAEFER, B.F., (1998). Palaeoproterozoic Kimban mobile belt, Eyre Peninsula; timing and significance of felsic and mafic magmatism and deformation. *Australian Journal of Earth Sciences* 45(2):305–313.

KOITCIN, N. (2010). Geodynamic Synthesis of the Gawler Craton and Curnamona Province. *Geoscience Australia, Record*(2010/27), 1-113

LAING, W. (1996). Stratigraphic subdivision of the Willyama Supergroup - Olary Domain, South Australia. *MESA Journal*(2), 39-48.

LUDWIG, K.R., & COOPER, J.A., (1984). Geochronology of Precambrian granites and associated U–Ti–Th mineralization, northern Olary province, South Australia. *Contributions to Mineralogy and Petrology* 86, 298–308.

MARJORIBANKS, R.W., RUTLAND, R.W.R., GLEN, R.A., LAING, W.P., (1980). The structure and tectonic evolution of the Broken Hill Region, Australia. *Precambrian Research* 13, 209–240.

MCAVANEY, S. O., JAGODZINSKI, E. A. AND PURVIS, A. C., (2012). Geochronology and geochemistry of a Kimban diorite, drillhole LED001, Lake Gilles, eastern Gawler Craton. *Geological Survey of South Australia*, RB 2012/10: 89.

*MCDONOUGH*, W.F. *& SUN*, S.S. (*1995*). Composition of the Earth. *Chemical Geology* 120: 223-253

MEDEIROS, S., WIEDEMANN-LEONARDOS, C., & VRIEND, S. (2001). Evidence of mingling between contrasting magmas in a deep plutonic environment: the example of Várzea Alegre, in

the Ribeira Mobile Belt, Espírito Santo, Brazil. *Anais Da Academia Brasileira De Ciências*, *73*(1), 99-119.

MORRISSEY L. J., HAND M., RAIMONDO T. & KELSEY D. E. (2014). Long-lived high-T, low-P granulite facies metamorphism in the Arunta Region, central Australia. *Journal of Metamorphic Geology* **32**, 25-47.

O'SULLIVAN, S. R., (2010). The Depositional and Clast Provenance Age of the Cppdnambana Metaconglomerate, Mount Woods Inlier. (Bachelor of Science), University of Adelaide, Unpublished.

OLIVER, R.L., AND FANNING, C.M., (1997). Australia and Antarctica; precise correlation of Palaeoproterozoic terrains, *in* Ricci Carlo, A., ed., The Antarctic region; Geological evolution and processes: Proceedings of the VII International Symposium on Antarctic Earth Sciences, Siena, Italy, *Terra Antarctica Publication*, p. 163–172.

OLLIER, C., (1967). Spheroical weathering, exfoliation and constant volume alteration. Z. *Geomorph*., 11, 103-108.

OZCHEM. Database: http://www.ga.gov.au/metadata-gateway/metadata/record/82426/.

PAGE, R.W., STEVENS, B.P.J., GIBSON, G.M., CONOR, C.H.H., (2000). Geochronology of Willyama Supergroup rocks between Olary and Broken Hill, and comparison to Northern Australia. In: Peljo, M.E. (Ed.), *Abstracts of Papers Presented at the May 2000 Conference in Broken Hill. Broken Hill, AGSO Record* 2000/10, pp.72–75.

PAGE, R.W., STEVENS, B.P.J., AND GIBSON, G.M., (2005). Geochronology of the sequence hosting the Broken Hill Pb-Zn-Ag orebody, Australia: *Economic Geology*, v. 100, p. 633–676.

PARKER, A.J., FANNING, C.M., FLINT, R.B., MARTIN, A.R., RANKIN, L.R., (1988). Archaean-early Proterozoic granitoids, metasediments and mylonites of southern Eyre Peninsula, South Australia: Specialist Group in Tectonics and Structural Geology, *Geological Society of Australia, Field Guide Series*, no. 2, 90 p.

PARKER, A.J., DALY, S.J., FLINT, D.J., FLINT, R.B., PREISS, W.V., TEALE, G.S., (1993). Palaeoproterozoic, *in* Drexel, J.F., Preiss, W.V., and Parker, A.J., eds., *The geology of South Australia; Volume 1, The Precambrian: South Australia Geological Survey, Bulletin* 54, p. 50–105.

PETFORD, N. (2003). Controls on primary porosity and permeability development in igneous rocks. *Geological Society, London, Special Publications*, *214*(1), 93-107.

RAETZ, M., KRABBENDAM, M., DONAGHY, A.G., (2002). Compilation of U–Pb zircon data from the Willyama Supergroup, Broken Hill region, Australia: evidence for three tectonostratigraphic successions and four magmatic events. *Australian Journal of Earth Sciences* 49, 965–983.

RAMSAY, J.G., (1962). Interference patterns produced by the superposition of folds of "similar" type. *Journal of Geology* 60, 466–481

RANKIN, L.R., FLINT, R.B., & FANNING, C.M., (1990). Palaeoproterozoic Nuyts Volcanics of the western Gawler craton, South Australia: *Department of Primary Industries and Resources, Report Book* 90/60, 17 p.

REID, A., & HAND, M., (2012). Mesoarchean to Mesoproterozoic evolution of the southern Gawler Craton, South Australia. *Episodes – News Magazine of the International Union of Geological Sciences*, 35, 216

REID, A. & JAGODZINSKI, E. A., (2012). PACE Geochronology: Results of collaborative geochronology projects 2011-12. *Department for Manufacturing, Innovation, Trade, Resources and Energy, South Australia, Adelaide*, Report Book 2012/00012: pp. 204.

REID, A. J., (2015). Zircon U-Pb geochronology from selected Paleoproterozoic igneous rocks of the Gawler Craton by laser ablation-inductively coupled plasma mass spectrometry. *Geological Survey of South Australia*, Report Book 2015/00025: 67 pp.

RUDNICK, R. (1992). Restites, Eu anomalies and the lower continental crust. *Geochimica Et Cosmochimica Acta*, *56*(3), 963-970.

SARIG. https://drillhole.pir.sa.gov.au/RockSampleSearchResults.aspx.

SNYDER, D., CRAMBES, C., TAIT, S., & WIEBE, R., (1997). Magma Mingling in Dikes and Sills. *The Journal Of Geology*, *105*(1), 75-86.

STEWART, J. R., & BETTS, P. G., (2010). Late Paleo–Mesoproterozoic plate margin deformation in the southern Gawler Craton: Insights from structural and aeromagnetic analysis. *Precambrian Research, 177*(1), 55-72. doi: 10.1016/j.precamres.2009.11.004

STEWART, K.P., & FODEN, J., (2003). Mesoproterozoic granites of South Australia: South *Australia Department of Primary Industries and Resources, Report Book*, 2003/15.

SWAIN, G., BAROVICH, K., HAND, M., FERRIS, G., SCHWARZ, M., (2008). Petrogenesis of the St Peter Suite, southern Australia: arc magmatism and Proterozoic crustal growth of the South Australian Craton: *Precambrian Research*, v. 166, pp. 283–296.

SYMINGTON, N. J., WEINBERG, R. F., HASALOVÁ, P., WOLFRAM, L. C., RAVEGGI, M., ARMSTRONG, R. A., (2014). Multiple intrusions and remelting-remobilization events in a magmatic arc: The St Peter Suite, South Australia. *GSA Bulletin*, 126: 1200–1218

SZPUNAR, M., HAND, M., BAROVICH, K., JAGODZINSKI, E., (2007). Age and Provenance of the Paleoproterozoic Hutchison Group, southern Gawler Craton, South Australia. Deformation in the Desert, Specialist Group in Tectonics and Structural Geology, *Geological Society of Australia, abstracts.*

TAYLOR, S.R, & MCLENNAN, S.M., (1995). The geochemical evolution of the continental crust. *Reviews of Geophysics* 33 (2), 241–265.

TEASDALE, J., (1997). Methods for understanding poorly exposed terranes: The interpretive geology and tectonothermal evolution of the western Gawler craton: Unpublished Ph.D. thesis, Australia, University of Adelaide, 183 p.

TOBISCH, O. & PATERSON, S. (1988). Analysis and interpretation of composite foliations in areas of progressive deformation. *Journal Of Structural Geology*, *10*(7), 745-754.

TWIDALE, C. & VIDAL ROMANÍ, J. (2005). *Landforms and geology of granite terrains*. Leiden, Netherlands: A.A. Balkema.

VERNON, R., ETHERIDGE, M., & WALL, V. (1988). Shape and microstructure of microgranitoid enclaves: Indicators of magma mingling and flow. *Lithos*, *22*(1), 1-11.

WADE, B., BAROVICH, K., & HAND, M., (2006). Evidence for early Mesoproterozoic arc-related magmatism in the Musgrave province, Australia: *Journal of Geology*, v. 114, p. 43–63.

WADE, C.E., (2011). Definition of the Mesoproterozoic Ninnerie Supersuite, Curnamona Province, South Australia, *MESA Journal*, 62, 25-42

WADE, C., REID, A., WINGATE, M., JAGODZINSKI, E., & BAROVICH, K., (2012). Geochemistry and geochronology of the c. 1585Ma Benagerie Volcanic Suite, southern Australia: Relationship to the Gawler Range Volcanics and implications for the petrogenesis of a Mesoproterozoic silicic large igneous province. *Precambrian Research*, *206-207*, 17-35.

WADE, C. E. & MCAVANEY, S., (2016). Palaeoproterozoic syn-tectonic magmatism on Eyre Peninsula: insights from new geochemistry and geochronology of the Peter Pan Supersuite. *Geological Society of Australia* Abstract No 118: 455.

WALTERS, A., GOODENOUGH, K., HUGHES, H., ROBERTS, N., GUNN, A., RUSHTON, J., LACINSKA, A., (2013). Enrichment of Rare Earth Elements during magmatic and post-magmatic processes: a case study from the Loch Loyal Syenite Complex, northern Scotland. *Contributions To Mineralogy And Petrology*, *166*(4), 1177-1202.

WINTER, J. (2010). Principles of igneous and metamorphic petrology, Second Edition, New York: *Prentice Hall.*

WURST, A. T. (1994). Analyses of late stage, Mesoproterozoic, syn and post tectonic, magmatic events in the Moonta Sub-domain: Implications for Cu-Au mineralisation in the "Copper Triangle" of South Australia. (Bachelor of Science), University of Adelaide.

ZANG, W. L. (2006). Maitland Special, South Australia, Map Sheets SI53-12 and portion SI53-16, *Geological Atlas 1:250 000 Series, Explanatory Notes. Geological Survey of South Australia*, Adelaide.

ZANG, W., FANNING, C.M., PURVIS, A.C., RAYMOND, O.L., BOTH, R.A., (2007). Early Mesoproterozoic bimodal plutonism in the southeastern Gawler Craton, South Australia: *Australian Journal of Earth Sciences*, v. 54, pp. 661–674.